

OUTP-99-50P
 Edinburgh 1999/16
 DAMTP-1999-138

Quenched QCD with $O(a)$ improvement: I. The spectrum of light hadrons

UKQCD Collaboration

K.C. Bowler, P. Boyle*, J. Garden, R.D. Kenway, D.G. Richards[†], P.A. Rowland,
 S.M. Ryan[‡], H. Simma

Department of Physics & Astronomy, University of Edinburgh, Edinburgh EH9 3JZ, Scotland

C. Michael

Department of Mathematical Sciences, University of Liverpool, Liverpool L69 3BX

H.P. Shanahan

DAMTP, University of Cambridge, 21 Silver Street, Cambridge CB3 9EW

H. Wittig

Theoretical Physics, 1 Keble Road, Oxford OX1 3NP

(July 11, 2018)

Abstract

We present a comprehensive study of the masses of pseudoscalar and vector mesons, as well as octet and decuplet baryons computed in $O(a)$ improved quenched lattice QCD. Results have been obtained using the non-perturbative definition of the improvement coefficient c_{sw} , and also its estimate in tadpole improved perturbation theory. We investigate effects of improvement on the

*present address: Department of Physics & Astronomy, University of Glasgow, Glasgow G12 8QQ

[†]present address: Jefferson Lab, 12000 Jefferson Avenue, Newport News, VA 23606, and Physics Department, Old Dominion University, Norfolk, VA 23529

[‡]present address: School of Mathematics, Trinity College, Dublin, Ireland

incidence of exceptional configurations, mass splittings and the parameter J . By combining the results obtained using non-perturbative and tadpole improvement in a simultaneous continuum extrapolation we can compare our spectral data to experiment. We confirm earlier findings by the CP-PACS Collaboration that the quenched light hadron spectrum agrees with experiment at the 10 % level.

PACS: 11.15.Ha, 12.38.Aw

I. INTRODUCTION

Despite recent efforts in simulating lattice QCD with dynamical quarks [1–3] the quenched approximation is still widely used. While precision tests of QCD through numerical simulations with dynamical quarks are not possible with the present generation of machines, accurate calculations of experimentally known quantities, such as the light hadron spectrum, can be performed using the quenched approximation. Recently the results of such a benchmark calculation using the Wilson fermion action have been presented by the CP-PACS Collaboration [4], superseding a similar study performed earlier by GF11 [5]. Results from a similar calculation employing staggered fermions were published in [6]. In ref. [4] it was concluded that the quenched light hadron spectrum deviates significantly from experiment by about 10%.

In order to reach this level of precision one needs to have control over many systematic effects, in particular lattice artefacts. In refs. [4,5] extrapolations to the continuum limit were performed, thus eliminating the dependence on the lattice spacing a . However, since the leading cutoff effects for Wilson fermions are linear in a , it is desirable to corroborate these findings and extend the analysis to weak hadronic matrix elements by performing a similar study using an improved action.

To leading order in a the Symanzik improvement programme amounts to adding the well-known Sheikholeslami-Wohlert term to the fermionic Wilson action [7]

$$\delta S = -c_{\text{sw}} \frac{i\kappa}{2} \sum_{x,\mu,\nu} \bar{\psi}(x) \sigma_{\mu\nu} F_{\mu\nu}(x) \psi(x). \quad (1)$$

Provided that c_{sw} is chosen appropriately, spectral quantities such as hadron masses approach the continuum limit with a rate proportional to a^2 . Non-perturbative determinations of c_{sw} have been performed in the quenched approximation [8,9] and for $n_f = 2$ flavours of dynamical quarks [10]. Estimates of c_{sw} in tadpole improved perturbation theory [11] are also widely used. Results for quantities in the light hadron sector using one or the other of the two methods have appeared recently [12–15,9,16–18].

In this paper we present results for the quenched light hadron spectrum in the continuum limit, using data computed for both non-perturbative and tadpole improved definitions of c_{sw} at several values of the lattice spacing. By combining the two datasets and performing a simultaneous continuum extrapolation, we obtain an independent check of the results reported in [4,5], using a different discretisation of the theory. Here we concentrate on the light hadron spectrum. Our results for weak matrix elements such as decay constants will be published elsewhere.

The main conclusion of this work is that the previously observed agreement of the quenched light hadron spectrum with experiment at the level of 10 %, is confirmed. Furthermore, we present qualitative and quantitative analyses of the effects of $O(a)$ improvement on mass splittings, the parameter J , the quark mass dependence of hadrons and the approach to the continuum limit. In many ways this work is a continuation of a previous paper [12].

The outline of the paper is as follows: in sect. II we present the details of our simulations, including the definition of improvement coefficients and our numerical procedures. Sections III and IV contain discussions of the “raw” results in the mesonic and baryonic

sectors, respectively. The quark mass dependence of hadron masses is discussed in sect. V. In sect. VI we present our results extrapolated to the continuum limit. Detailed comparisons of our results and conclusions are presented in sect. VII.

II. DETAILS OF THE SIMULATION

A. Improvement coefficients and simulation parameters

We have generated gauge field configurations using the Wilson plaquette action at three values of $\beta = 6/g_0^2$, namely $\beta = 5.7, 6.0$ and 6.2 . We used the same hybrid over-relaxed algorithm described in [19]. For the fermions we have used the $O(a)$ improved Wilson action defined by

$$S_F^{\text{impr}}[U, \bar{\psi}, \psi] = S_F^W[U, \bar{\psi}, \psi] - c_{\text{sw}} \frac{i\kappa}{2} \sum_{x, \mu, \nu} \bar{\psi}(x) \sigma_{\mu\nu} F_{\mu\nu}(x) \psi(x), \quad (2)$$

where S_F^W is the standard Wilson action and $F_{\mu\nu}$ is a lattice definition of the field strength tensor. The improvement coefficient c_{sw} has been calculated to one loop in perturbation theory [20,21]

$$c_{\text{sw}} = 1 + 0.267 g_0^2 + O(g_0^4). \quad (3)$$

It has also been determined non-perturbatively for $\beta \geq 6.0$ in ref. [8] and for $\beta \geq 5.7$ in [9].

We have computed quark propagators at $\beta = 6.0$ and 6.2 , using the non-perturbative determination of c_{sw} from [8]

$$c_{\text{sw}}^{\text{np}} = \frac{1 - 0.656g_0^2 - 0.512g_0^4 - 0.054g_0^6}{1 - 0.922g_0^2}, \quad \beta \geq 6.0. \quad (4)$$

Furthermore we have used tadpole improved tree-level estimates for c_{sw} ,

$$c_{\text{sw}}^{\text{tad}} = u_0^{-3}, \quad u_0^4 = \frac{1}{3} \langle \text{Re Tr } U_P \rangle, \quad (5)$$

in order to calculate quark propagators at $\beta = 5.7, 6.0$ and 6.2 . In the following we shall refer to the datasets computed using either $c_{\text{sw}}^{\text{np}}$ or $c_{\text{sw}}^{\text{tad}}$ as NP and TAD, respectively.

Our values for the hopping parameter κ were chosen such that they straddle the region of the strange quark mass. The simulation parameters for each dataset are compiled in Table I, which also contains the estimates of the spatial extensions for each lattice in physical units. Exceptional configurations which were encountered at $\beta = 6.0$ for $c_{\text{sw}}^{\text{np}}$ have been removed from the statistical ensemble. The incidence of those configurations is examined in more detail in subsect. II C.

In ref. [22] it was argued that the bare parameters have to be rescaled in the $O(a)$ improved theory, so that spectral quantities approach the continuum limit with a rate proportional to a^2 .¹ In the quenched approximation the rescaling needs to be performed only for the bare (subtracted) quark mass

$$m_q = \frac{1}{2a} \left(\frac{1}{\kappa} - \frac{1}{\kappa_c} \right), \quad (6)$$

where κ_c is the critical value of the hopping parameter. The rescaled quark mass \widetilde{m}_q is defined by

$$\widetilde{m}_q = m_q (1 + b_m a m_q), \quad (7)$$

and the improvement coefficient b_m has been computed in one-loop perturbation theory as [23]

$$b_m = -\frac{1}{2} - 0.0962 g_0^2 + O(g_0^4). \quad (8)$$

So far b_m has been determined non-perturbatively only at $\beta = 6.2$ [24]. We have thus used the perturbative estimate in eq. (8), evaluated with a “boosted” coupling $g^2 = g_0^2/u_0^4$ unless stated otherwise. In practice we found that the details in the evaluation of b_m (e.g. bare versus boosted perturbation theory) have little influence on our results.

B. Hadron correlators and fitting procedure

Our quark propagators were calculated using both local and smeared sources and sinks. The smearing was performed using either the “fuzzing” technique described in ref. [25] or the Jacobi smearing algorithm of ref. [26]. Both smearing procedures are gauge invariant. They also have a number of parameters, which can be tuned in order to optimise the projection on a given hadronic state. For Jacobi smearing the projection properties are controlled by the parameter κ_S , which appears in the kernel of the smearing operator, and the number of iterations, N_{jac} [26]. Based on our experience we always chose $\kappa_S = 0.25$ and used N_{jac} to control the smearing radius.

The fuzzing algorithm for hadronic correlators has three tunable parameters, denoted by c , N_{fz} and r . The parameter c is the so-called “link-staple mixing ratio”, which appears in the construction of fuzzed spatial links (at fuzzing level n) according to [27]

$$U_j^{(n)}(x) = \mathcal{P} \left\{ c U_j^{(n-1)}(x) + \sum_{k=\pm 1, k \neq j} U_k^{(n-1)}(x) U_j^{(n-1)}(x + \hat{k}) U_k^{(n-1)\dagger}(x + \hat{j}) \right\}, \quad (9)$$

¹The rescaling is required if a mass independent renormalisation scheme is adopted in which all renormalisation conditions are imposed at zero quark mass. In order for such a scheme to be compatible with $O(a)$ improvement the renormalisation of the bare parameters cannot be avoided.

where \mathcal{P} denotes the projection back into the group manifold of $SU(3)$. The maximum number of fuzzing levels is given by N_{fz} . Throughout this work we have used $c = 2$ and $N_{\text{fz}} = 5$. The size of the fuzzed source (sink) is then determined by r , which is simply the length of the straight path of fuzzed links emanating from the origin into all (positive and negative) spatial directions.

An extensive investigation into the optimal smearing parameters, using the projection on both mesonic and hadronic states, was performed at $\beta = 6.0$ on $16^3 \cdot 48$ for $c_{\text{sw}}^{\text{np}}$ [28]. It was found that $N_{\text{jac}} = 16$ turned out to be a compromise between good projection properties and acceptable noise levels in all types of correlators. Similarly, the optimal radius for fuzzed sources was determined to be $r = 6$. For different β -values the radius r was scaled with the lattice spacing. The type of smearing and the corresponding values of N_{jac} or r are listed in Table I for all datasets.

Quark propagators computed using smeared or local sources/sinks were combined into hadron correlators. We always use the generic notation 'S' to denote correlators which have been smeared, regardless of whether fuzzing or Jacobi smearing was used to smear the sources and/or sinks. By 'L' we denote unsmeared ("local") sources and sinks. For instance, meson and baryon correlators which have been smeared at the source but not at the sink are both labelled 'SL' in this notation. The generalisation to other combinations of source and sink smearing is obvious.

We have computed meson and baryon correlators for degenerate and non-degenerate combinations of quark masses. Meson correlators in the pseudoscalar and vector channels were analysed, as well as spin-1/2 (octet) and spin-3/2 (decuplet) baryons.

Our meson masses were extracted by performing correlated, simultaneous fits to the (LL, SS) or (LL, SL) combination of correlators. In most cases we used a double-cosh formula to fit the ground state and the first excitation, requiring the masses in the fit formulae to coincide for both the LL and SS (or SL) correlators. At $\beta = 6.0$ on $32^3 \cdot 64$ the double-cosh fits turned out to be unstable, so that we resorted to single-cosh fits to either the SS or SL correlator. For baryons we followed the same strategy, using double-exponential fits, and, at $\beta = 6.0$, $32^3 \cdot 64$, a single exponential.

All fitting intervals have been determined by performing a "sliding window" analysis, in which we first selected the maximum timeslice, t_{max} , of the fitting interval (usually $t_{\text{max}} \lesssim T/2$) and then pushed t_{min} to its lowest value which was compatible with the requirements of low χ^2/dof and overall stability of the fitted masses.

All statistical errors have been estimated using the bootstrap method with 1000 bootstrap samples. More details about our implementation of the method can be found in [29].

C. Exceptional configurations

It has been noted that calculations of fermionic quantities occasionally suffer from abnormally large fluctuations, in particular for small quark masses [30,8]. These fluctuations have been linked to exceptionally small eigenvalues of the Dirac operator, and the gauge configurations on which they occur are usually called "exceptional configurations". The fraction of such configurations in the total statistical ensemble increases for smaller quark mass m_q and/or larger values of g_0^2 , c_{sw} and the lattice volume [8].

In our simulations we have encountered exceptional configurations at $\beta = 6.0$, but not at the other two β -values. In order to compare their incidence for $c_{\text{sw}}^{\text{tad}}$ and $c_{\text{sw}}^{\text{np}}$ we have analysed distributions of observables for $\beta = 6.0$ on $16^3 \cdot 48$, using the smallest quark mass in the TAD and NP datasets. The chosen observable was the unsmeared (i.e. LL) pseudoscalar correlator at $t = T/2$.

To this end we have determined the median x_m and the values denoting the upper (x_u) and lower (x_l) ends of the central 68 %. As a measure for the width one can define the ratio

$$\frac{\Delta x_u}{x_m}, \quad \Delta x_u = x_u - x_m. \quad (10)$$

The distributions are quite similar for the TAD and NP datasets. First, their width is comparable, since $\Delta x_u/x_m \approx 0.65$ in both cases. Second, both distributions extend smoothly out to about $x_m + 9\Delta x_u$.

There are, however, differences in the tails of the distributions, i.e. the number of values encountered far beyond $x_m + 9\Delta x_u$. In the TAD dataset only one configuration is encountered, which produces a value at roughly $37\Delta x_u$ above the median, whereas in the NP dataset there are three such configurations with values for the pseudoscalar correlator at $44\Delta x_u$, $65\Delta x_u$ and $360\Delta x_u$ above x_m .

We draw two conclusions from this analysis. The fact that the width is comparable (i.e. the value of $\Delta x_u/x_m$) suggests that the typical statistical fluctuations do not increase significantly as c_{sw} is increased from its tadpole improved perturbative estimate to the non-perturbative value. Second, we have confirmed the increase of the fraction of exceptional configurations (i.e. those configurations for which the observable shoots up to values which are orders of magnitude above the normal level of fluctuations) for larger c_{sw} . The presence of a zero eigenvalue of the Dirac operator at a nearby κ -value has also been verified for such configurations [32].

We did not make attempts to treat exceptional configurations using, for instance, the methods described in [31]. Instead we have chosen to eliminate them from our statistical ensemble. That is, at $\beta = 6.0$, $16^3 \cdot 48$ we have removed the two configurations which produced the most extreme values in the distribution of the unsmeared pion propagator for $c_{\text{sw}}^{\text{np}}$, and on which the inversion of the Dirac operator did not converge for some of its components. The latter also occurred on another configuration if a fuzzed source was used, and that configuration was subsequently removed as well. The total number of exceptional configurations which were removed for a particular dataset are shown in brackets in Table I. Note that no configurations were eliminated from the TAD datasets.

For our range of β -values and the corresponding values of c_{sw} the incidence of exceptional configurations is still relatively small. Their fraction in the NP dataset amounts to less than 1% on $16^3 \cdot 48$ (3% on $32^3 \cdot 64$), and after the analysis presented here we do not expect serious distortions of the statistical ensembles due to their removal.

III. RESULTS FOR PSEUDOSCALAR AND VECTOR MASSES

In Tables II–V we present our “raw” results for meson masses in the pseudoscalar and vector channels, which were obtained from the fits described in the previous section. The

fit ranges were determined independently for the (LL,SL) and (LL,SS) combinations of correlators. Both combinations gave consistent results, and in general we quote the result from the fit which gave the best value of χ^2/dof .

In the pseudoscalar channel the fits were very stable under variations of the fitting interval. By contrast, the fits in the vector channel could in some cases differ by up to one standard deviation if a different fitting interval was selected. We estimate the systematic error in the mass of the vector meson arising from choosing alternative fitting ranges to be at most as large as the statistical error. This systematic error has not been included in the tables.

A. Finite volume effects

Based on our results for the NP dataset obtained at $\beta = 6.0$ on $16^3 \cdot 48$ and $32^3 \cdot 64$, we can make a first estimate of finite size effects in the mesonic sector. In physical units the spatial extensions of the two lattices correspond to $L \approx 1.5$ fm and 3.0 fm, respectively.

In the pseudoscalar channel we find evidence for small but significant finite volume effects. On the smaller lattice the values for am_{PS} are consistently larger. Furthermore, the effect shows a trend to increase as the quark mass gets smaller. Both these observations are consistent with the expected qualitative features of finite-size effects. The difference in am_{PS} determined for the two lattice sizes amounts to 0.6% at the largest and 1.5% at the smallest quark mass. At all values of κ the deviation is a two- σ effect.

By contrast, no statistically significant finite size effects are observed in the vector channel. In fact, the values for am_V are slightly higher on the larger lattice. This might be attributed to the fact that no estimate for contributions from excited states was available for all hadron masses computed on $32^3 \cdot 64$, since only single-cosh fits could be performed. Indeed, one of the caveats in the analysis of finite volume effects in both channels is the fact that the data for the two lattice sizes shown in Tables II and III have not been obtained using the same fitting procedure. We have, therefore, repeated the analysis for the smaller volume, by performing single-cosh fits for appropriately chosen intervals. The results are consistent with those shown in the tables. However, in the pseudoscalar channel it is also possible to choose small fitting intervals close to t_{max} such that the single-cosh fits on $L \approx 1.5$ fm produce smaller values with larger errors, which are both compatible with the results in the tables and also with those obtained on the larger volume. We conclude that the finite size effects observed in the pseudoscalar channel appear to be genuine, but without further investigations one cannot rule out entirely that they have a statistical origin. For vector mesons no significant effects are observed.

B. Vector-pseudoscalar mass splitting

It has been known for some time that lattice results obtained in the quenched approximation fail to reproduce the experimental fact that the vector-pseudoscalar hyperfine splitting is constant over a wide range of quark masses, i.e. $m_V^2 - m_{\text{PS}}^2 \approx 0.55 \text{ GeV}^2$. Indeed, lattice estimates for this quantity are in general much lower when unimproved Wilson fermions are employed.

In order to study the effect of $O(a)$ improvement on the hyperfine splitting we have plotted our results for the NP and TAD datasets in Fig. 1 (a) and (b), respectively. In order to display the influence of finite lattice spacing, we have expressed our results in units of the hadronic radius r_0 [33], using its lattice determination in ref. [34]. The figure demonstrates that with improvement (either non-perturbative or mean field) the hyperfine splittings show much weaker variation over the studied range of quark masses, compared to the unimproved case (see, e.g. ref. [19]). However, the small slope in the data for $r_0^2(m_V^2 - m_{PS}^2)$ as a function of $(r_0 m_{PS})^2$ suggests that the experimentally observed *very* weak dependence on the quark mass is not reproduced by the lattice data.

By comparing the NP and TAD datasets it appears that the dependence on the lattice spacing is somewhat smaller for non-perturbative c_{sw} . Of course this needs to be corroborated in a real scaling analysis at a fixed value of $(r_0 m_{PS})^2$.

At first sight it may seem surprising that the lattice results for the hyperfine splitting overestimate the experimentally observed values. However, lattice results for the splittings in the quenched approximation in physical units depend strongly on the choice of scale. Indeed, if the scale is set using m_K the lattice values are much closer to experiment [35,28]. However, the main focus of this discussion is the analysis of the dependence on the quark mass and the lattice spacing.

C. The parameter J

The parameter J was introduced [36] as a means to detect deviations between the quenched approximation and the observed hadron spectrum without relying on chiral extrapolations. It is defined through

$$J = m_V \frac{dm_V}{dm_{PS}^2}, \quad m_V/m_{PS} = m_{K^*}/m_K, \quad (11)$$

and is thus related closely to the slope of the vector-pseudoscalar splitting discussed above. Its phenomenological value has been determined from the experimentally measured masses as $J = 0.48(2)$.

In Fig. 2 we plot our results for all our datasets as a function of the lattice spacing. Our values confirm previous observations that J is underestimated in the quenched approximation. In fact, one finds that the low values for J have little to do with lattice artefacts, since there is no sign of the data approaching the phenomenological value for J in the continuum limit. We conclude that low lattice estimates for J appear to be an intrinsic feature of the quenched approximation.

IV. RESULTS FOR OCTET AND DECUPLET BARYONS

Our results for masses of octet and decuplet baryons are shown in Tables VI–XII. They have been obtained by performing double-exponential fits to the (LL,SS) or (LL,SL) combination of baryon correlation functions, except on $32^3 \cdot 64$ for the NP dataset at $\beta = 6.0$, where – in analogy to the fits of the large-volume data in the mesonic sector – only single exponential fits to smeared correlators were considered.

Tables VI and VII contain the results for baryon masses in the nucleon ($J^P = \frac{1}{2}^+$) and Δ ($J^P = \frac{3}{2}^+$) channels for degenerate combinations of quark masses, together with the fitting ranges and the values of χ^2/dof . These results can be extrapolated to the physical values of the quark masses in order to determine the masses of the nucleon, the $\Delta(1232)$ and the $\Omega(1672)$, as described in sect. V.

A. Baryons for non-degenerate quark masses

In order to compute the masses of the physical Λ , Σ and Ξ states one has to consider baryon correlators for non-degenerate combinations of quark masses. In the octet sector one has to distinguish between “ Σ -like” and “ Λ -like” correlators. Using the generic notation u, d, s to denote quark flavours, we note that Σ -like states are symmetric in the light flavours u, d , whereas Λ -like states are antisymmetric. On the lattice the corresponding correlators are obtained by performing the appropriate contractions [37,38,28]. The $J^P = \frac{1}{2}^+$ states of the Σ and Λ are then obtained from the correlation functions by averaging the 11 and 22 spinor indices.

The correlators for decuplet baryons, which are symmetric in all flavours u, d, s are simpler to construct. They are obtained in terms of the interpolating operator

$$D_{\mu;ijk} = \epsilon_{abc} \left(\psi_i^a C \gamma_\mu \psi_j^b \right) \psi_k^c, \quad (12)$$

where i, j, k denote the quark flavour, a, b, c are colour indices, and C is the charge conjugation matrix. Correlation functions for decuplet baryons are constructed from the correlation of $D_{\mu;ijk}$ by projecting out the spin- $\frac{3}{2}$ component.

In Tables VIII–XII we list the results for octet (Σ , Λ -like) and decuplet (Δ -like) baryons for non-degenerate combinations of quark masses. The fitting intervals, which are not shown, are mostly identical to those chosen for the corresponding channels in the degenerate case (Tables VI and VII). With our statistical accuracy we are not able to distinguish between Σ - and Λ -like states; the different symmetry properties in the quark flavours corresponding to the hopping parameters κ_1 and κ_2 do not manifest themselves in statistically significant mass differences.

By extrapolating or interpolating the data in $\kappa_1, \kappa_2, \kappa_3$ to the hopping parameters corresponding to the physical quark masses one obtains the masses of the $\Lambda, \Sigma, \Sigma^*, \Xi, \Xi^*$ and Ω . Note that non-degenerate combinations of quark masses have not been computed at $\beta = 5.7$.

B. Finite volume effects in the baryonic sector

The issue of finite-volume effects is of special importance in the baryonic sector where these effects are expected to be more severe than for mesons. With our data we can assess the influence of finite-volume effects by comparing our results computed at $\beta = 6.0$ on either $16^3 \cdot 48$ or $32^3 \cdot 64$ using the non-perturbative value of c_{sw} .

The numbers in Tables VI, VIII and IX suggest that on the large volume the mass estimates for both octet and decuplet baryons are slightly smaller. For octet baryons this decrease amounts to about 1.4% at the largest and 2.7% at the smallest quark masses. The

effect is roughly twice as large as for the pseudoscalar mesons discussed earlier. Although finite-size effects for octet baryons are not significant at our level of statistical accuracy, this does not necessarily indicate that those effects are absent.

For decuplet baryons the finite-volume effects are more pronounced; they vary between 2.4 and 5.5%, again increasing towards smaller quark masses. Here the discrepancy between the results on the small and large volumes amounts to about 1.5 standard deviations. Thus we cannot exclude finite-size effects in our baryon data at a level of up to 2.5% for octet and 5.5% for decuplet baryons.

V. QUARK MASS DEPENDENCE

In this section we discuss the dependence of mesons and baryons on the quark mass. Usually this dependence is modelled using the results of chiral perturbation theory at lowest order. It is then quite a delicate problem to decide whether higher orders in the chiral expansion have to be included. Furthermore, additional care must be taken in the quenched approximation, where one expects deviations from the leading behaviour for very small quark masses (i.e. close to the chiral limit), due to the appearance of quenched chiral logarithms [39,40,37,41]. We will first motivate the functional forms for the quark mass dependence used in this paper, determine the critical hopping parameter and then present our results for hadron masses extrapolated or interpolated to the physical quark masses.

A. Fit ansatz and the critical hopping parameter

Usually the critical value of the hopping parameter, κ_c , is determined at the point where the mass of the pseudoscalar meson vanishes, $m_{\text{PS}} = 0$. The simplest ansatz for the quark mass dependence of m_{PS} , which is consistent with $O(a)$ improvement, is

$$m_{\text{PS}}^2 = B(\widetilde{m}_{\text{q},1} + \widetilde{m}_{\text{q},2}), \quad (13)$$

where $\widetilde{m}_{\text{q},i}$, $i = 1, 2$ denotes the rescaled, bare quark mass defined in eq. (7).

Assuming that the ansatz in eq. (13) is justified (i.e. both higher orders in the quark mass as well as quenched chiral logarithms are assumed to be absent), we have determined κ_c using both degenerate and non-degenerate combinations of quark masses, by inserting the definition of \widetilde{m}_{q} into eq. (13), which leads to the general fit ansatz

$$m_{\text{PS}}^2 = \alpha + \beta \left(\frac{1}{\kappa_1} + \frac{1}{\kappa_2} \right) + \gamma \left(\frac{1}{\kappa_1^2} + \frac{1}{\kappa_2^2} \right), \quad (14)$$

where the fit parameters α , β and γ are related to B , κ_c and b_{m} through

$$\alpha = \frac{B}{\kappa_c} \left(-1 + \frac{b_{\text{m}}}{2\kappa_c} \right), \quad \beta = \frac{B}{2} \left(1 - \frac{b_{\text{m}}}{\kappa_c} \right), \quad \gamma = \frac{Bb_{\text{m}}}{4}. \quad (15)$$

As mentioned in sect. II we have used the tadpole improved perturbative estimate at one loop for b_{m} . In order to study the sensitivity of κ_c on b_{m} we have also used its estimate in

one-loop perturbation theory in the bare coupling, as well as its tree-level value, $b_m = -1/2$, and, at $\beta = 6.2$ for the NP dataset, the non-perturbative determination of ref. [24]. In order to enable direct comparisons with κ_c -estimates from earlier simulations using tadpole improvement, we have also computed κ_c for $b_m = 0$ for the TAD dataset. Our results, which are collected in Table XIII, show little dependence on the value of b_m . The largest deviations are observed at $\beta = 5.7$. Furthermore, using the non-perturbative value of b_m at $\beta = 6.2$ yields a result which is entirely compatible with the ones obtained using one-loop perturbative estimates.

We conclude that for our range of quark masses, estimates for b_m based on one-loop perturbation theory are sufficient to obtain stable results for κ_c for $\beta \gtrsim 6.0$.

We can now justify our ansatz eq. (13) by plotting m_{PS}^2 as a function of $(\widetilde{m}_{q,1} + \widetilde{m}_{q,2})/2$ in units of r_0 for both NP and TAD datasets. This is shown in Fig. 3 where the lines denote the fits based on eq. (13). The plots show that no significant departure from the linear behaviour predicted by lowest order chiral perturbation theory is observed in the range of quark masses investigated. Thus, we find no evidence for higher order terms in the chiral expansion of m_{PS}^2 , nor do our data support the presence of quenched chiral logarithms. The latter is most probably due to the fact that the quark masses used in our simulations are not light enough.

Furthermore, we wish to point out that a more sophisticated analysis [18] of the quark mass dependence of the data in Table II revealed that higher-order terms proportional to $(\widetilde{m}_{q,1} - \widetilde{m}_{q,2})^2$ contribute below the 1% level.

Based on our observations in the pseudoscalar channel, which usually offers the most precise information about the quark mass dependence, we have used the following functional forms for vector mesons, octet and decuplet baryons:

$$m_V = A_V + C_V (\widetilde{m}_{q,1} + \widetilde{m}_{q,2}) \quad (16)$$

$$m_{\text{Oct}} = A_O + C_O (\widetilde{m}_{q,1} + \widetilde{m}_{q,2} + \widetilde{m}_{q,3}) \quad (17)$$

$$m_{\text{Dec}} = A_D + C_D (\widetilde{m}_{q,1} + \widetilde{m}_{q,2} + \widetilde{m}_{q,3}). \quad (18)$$

The corresponding fits are shown in Figs. 4 and 5 for the NP and TAD datasets, respectively. As in the case of pseudoscalar mesons we observe that for our level of precision and range of quark masses there is no evidence for curvature in the data. We conclude that eqs. (13–18) represent appropriate fitting functions for our data. A detailed analysis of more complicated models for the quark mass dependence described in [28] resulted in similar findings.

In a given channel (i.e. pseudoscalar and vector mesons, Σ -, Λ - and Δ -like baryons) we have determined the parameters B , A_V , C_V , ... from uncorrelated, simultaneous fits to degenerate and non-degenerate combinations of quark masses. The only exception was the dataset at $\beta = 5.7$, for which only two degenerate combinations of quark masses had been computed in the baryonic channels. Therefore, the quark mass dependence at $\beta = 5.7$ is not really controlled. Nevertheless, we have included the results in the following analysis.

B. Hadrons at physical values of the quark masses

Our task now is to make contact with the physical hadron spectrum by matching the quark masses in eqs. (13–18) to the masses of the physical u , d and s quarks. Here we employ

the axial Ward identities, which, for the physical pseudoscalar mesons (in the continuum theory), read

$$m_{\pi^\pm}^2 = B(m_u + m_d) \quad (19)$$

$$m_{K^\pm}^2 = B(m_u + m_s), \quad m_{K^0}^2 = B(m_d + m_s). \quad (20)$$

By assuming isospin symmetry, i.e. $m_u = m_d$ one can define the so-called “normal” quark mass m_n through

$$m_n \equiv \frac{1}{2}(m_u + m_d) \quad (21)$$

and the isospin-averaged combination of kaon masses as

$$m_K^2 \equiv \frac{1}{2}(m_{K^\pm}^2 + m_{K^0}^2), \quad (22)$$

such that

$$m_{\pi^\pm}^2 = 2B m_n \quad (23)$$

$$m_K^2 = B(m_n + m_s). \quad (24)$$

Inserting $m_{K^\pm}^2 = 493.7 \text{ MeV}$ and $m_{K^0} = 497.7 \text{ MeV}$ [42] one obtains²

$$m_K = 495.7 \text{ MeV}. \quad (25)$$

Using our lattice estimates for the parameter B we can determine the combination of (bare) quark masses $\widetilde{m}_s + \widetilde{m}_n$ and the quark mass \widetilde{m}_n through

$$a(\widetilde{m}_s + \widetilde{m}_n) = (aQ)^2 \frac{(m_K/Q)_{\text{phys}}^2}{aB} \quad (26)$$

$$a\widetilde{m}_n = (aQ)^2 \frac{(m_\pi/Q)_{\text{phys}}^2}{2aB}, \quad (27)$$

where Q is the quantity which sets the lattice scale, and the subscript “phys” denotes that the physical ratio is to be taken. It is a well-known fact that in the quenched approximation there is an intrinsic ambiguity associated with the lattice scale. In order to estimate this ambiguity we have used three different quantities for Q , namely

$$\begin{aligned} Q &= r_0^{-1}, \quad r_0 = 0.5 \text{ fm}, \quad r_0^{-1} = 395 \text{ MeV}, \\ Q &= m_{K^*}, \quad m_{K^*} = 893.9 \text{ MeV}, \\ Q &= m_N, \quad m_N = 938 \text{ MeV}. \end{aligned} \quad (28)$$

Here, the value $m_{K^*} = 893.9 \text{ MeV}$ is the isospin averaged result, i.e. $m_{K^*} = \frac{1}{2}(m_{K^{*\pm}} + m_{K^{*0}})$. Lattice data for r_0/a and its error at all relevant β -values were taken from ref. [34]. In particular, we used the interpolating formula, eq. (2.18) of [34].

The following comments apply to our chosen set of lattice scales:

²In principle one also has to compensate for the electromagnetic binding energy of about -0.7 MeV in eq. (25) (see e.g. ref. [18]). However, this has not been done in this paper.

- On the lattice the mass of the K^* meson is obtained through an interpolation of data points, which is intrinsically a safe procedure. However, the physical K^* is an unstable hadron with a finite width; resonance effects are not controlled in the lattice calculation;
- The nucleon is a stable hadron, but in lattice simulations its mass is obtained only by an extrapolation close to the chiral limit. In view of the possible presence of quenched chiral logarithms this extrapolation is hard to control. Furthermore, precise lattice determinations of baryon masses are more difficult compared to the mesonic sector, due to larger statistical errors and the possibility of relatively large finite size effects;
- The hadronic radius r_0 is known accurately for a wide range of lattice spacings [34], but a direct experimental measurement is not available. Its phenomenological value of $r_0 = 0.5 \text{ fm}$ is estimated from potential models fitted to experimental data.

In Table XIV we have collected the results for the hopping parameters κ_n and κ_s , corresponding to the quark masses $a\widetilde{m}_n$ and $a\widetilde{m}_s$, obtained for our three different choices of Q and using the tadpole improved perturbative estimate for b_m in the definition of $a\widetilde{m}_q$. Thus, in spite of the difficulties associated with extrapolations to the chiral limit we have chosen to compute $a\widetilde{m}_n$ and to quote lattice estimates for m_ρ , m_N and m_Δ .

The physical vector meson, octet and decuplet baryon masses have been computed by inserting the appropriate combinations of $a\widetilde{m}_n$ and $a\widetilde{m}_s$, corresponding to the physical quark content, into eqs. (16–18). The results, in units of either r_0 , m_{K^*} or m_N are shown in Tables XV, XVI and XVII, respectively. These tables contain the data with $L/a \leq 24$ only. For completeness, the non-perturbatively improved data obtained on $32^3 \cdot 64$, $\beta = 6.0$, which have not been used in the continuum extrapolation, are listed in Table XVIII.

It has been observed that several tests of the quenched approximation can be performed at intermediate values of the quark mass (e.g. near the strange quark mass), so that extrapolations to the chiral limit as a reference point are not required [36]. Furthermore, it has been suggested that properties of the effective chiral Lagrangian can be studied for *unphysical* quark masses. A convenient reference point for future lattice studies is then provided by the condition $(m_{\text{PS}}r_0)^2 = 3.0$, which has already been chosen in ref. [18]. We have interpolated our results in the vector meson, Σ and Δ channels to that point by defining a reference quark mass $\widetilde{m}_{\text{ref}}$ through

$$2(aB)(a\widetilde{m}_{\text{ref}})(r_0/a)^2 = 3.0 \quad (29)$$

and inserting its value into eqs. (16–18). The results are shown in Table XIX.

Another reference point which does not require extrapolations to the chiral limit is defined at the point where

$$m_{\text{PS}}/m_V = 0.7. \quad (30)$$

Results for the vector meson and nucleon masses at the reference point defined by eq. (30) have been quoted in [14,9]. Our estimates in the vector, Σ and Δ channels are included in Table XIX. By comparing the results in Tables XIX and XV one observes that both reference points correspond to the case of degenerate light quarks with masses around that of the strange quark.

VI. THE CONTINUUM LIMIT

We are now in a position to discuss the extrapolation of our results to the continuum limit. This will finally enable us to make a direct comparison with experimental data and the results of ref. [4], obtained using the unimproved Wilson action.

For hadron masses computed using the non-perturbative determination of c_{sw} the leading cutoff effects are expected to be of order a^2 . Detailed scaling studies have confirmed that the approach to the continuum limit for spectral quantities [9,43] and matrix elements [43] is indeed consistent with such a leading order. By contrast, it is expected that small terms of order a cannot be excluded when tadpole improvement is used [14].

From our list of simulation parameters in Table I it is clear that separate continuum extrapolations of the results for the NP and TAD datasets are not feasible. We have therefore chosen to perform simultaneous extrapolations by assuming leading lattice artefacts of order a^2 for the NP and artefacts of both order a and a^2 for the TAD dataset. The ansatz for the continuum extrapolation of a generic hadron mass M in units of r_0 then reads

$$r_0 M = \begin{cases} r_0 M|_{a=0} + B^{\text{NP}}(a/r_0)^2 \\ r_0 M|_{a=0} + A^{\text{TAD}}(a/r_0) + B^{\text{TAD}}(a/r_0)^2. \end{cases} \quad (31)$$

In other words, one requires that the data computed for non-perturbative and tadpole improvement extrapolate to a common continuum value. By combining the results obtained at three β -values for tadpole improvement with those at two β -values in the case of non-perturbative improvement we have five data points to determine the four fit parameters $M, B^{\text{NP}}, A^{\text{TAD}}$ and B^{TAD} . Note that the data obtained on $32^3 \cdot 64$ at $\beta = 6.0$ have not been used. It is worth pointing out that the spatial volume at $\beta = 5.7$ is larger than those for the larger two β -values which enter the extrapolations.

In Fig. 6 we show examples of continuum extrapolations based on eq. (31), namely one representative of each of the vector meson, octet and decuplet baryon channels, respectively. The extrapolations have been repeated for the other two choices of the lattice scale, i.e. $Q = m_{K^*}$ and m_N . The value of χ^2/dof for these fits was quite low (below 1) for all channels considered.

The results are listed in Tables XV–XVII in the row labelled “Cont.”. These numbers represent the final results for the physical hadrons in this paper. In addition we have also performed continuum extrapolations of hadrons interpolated to $(m_{\text{PS}}r_0)^2 = 3.0$. The results are also included in Table XIX.

To check whether or not the continuum extrapolations for different choices of the lattice scale are controlled, one can compare, for instance, the continuum result for a particular hadron in units of m_{K^*} , i.e. (M/m_{K^*}) with the ratio $(r_0 M)/(r_0 m_{K^*})$. It then turns out that not only are the values consistent within errors, but they are also numerically very close. This gives us further confidence that the continuum estimates in Tables XV–XVII are reliable.

From the results in the tables one can also estimate the size of lattice artefacts at a fixed β -value, say, $\beta = 6.0$ which roughly corresponds to $a \approx 0.1 \text{ fm}$. Using the numbers from Table XV one infers that lattice artefacts for both mesons and baryons at $\beta = 6.0$ are of the order of 5 % or less. Apart from Tables XV–XIX and Fig. 6 some information about the

relative scaling behaviour of the NP and TAD datasets can also be gained from Figs. 3–5. Here one observes that data for mesons and baryons in units of r_0 are almost independent of the lattice spacing for $\beta \geq 6.0$. This is particularly pronounced when non-perturbative improvement is employed. It is also clear that significant lattice artefacts are present in the tadpole improved data at $\beta = 5.7$.

VII. DISCUSSION AND CONCLUSIONS

Our final results in Tables XV–XVII and XIX can now be compared to other lattice calculations and experimental data.

In ref. [18] results for vector mesons computed using the non-perturbative value of c_{sw} were presented. By comparing our results for $r_0 m_V$ computed at $(r_0 m_{\text{PS}})^2 = 3.0$ and those for $r_0 m_{K^*}$ to ref. [18] we find differences of 1–2 standard deviations at most. Since the numerical procedures employed in [18] are quite different to those used in this paper (see also [17]) this agreement is an important check of the stability of our results, both at finite lattice spacing and in the continuum limit.

As mentioned in the introduction, one important goal of this study is to corroborate earlier findings by GF11 [5] and the CP-PACS Collaboration [4], using an improved discretisation of the QCD action. In Fig. 7 we present our final results in physical units, computed using either m_{K^*} or m_N to set the scale. Our numbers are compared to the CP-PACS results, obtained using m_ρ to set the scale, and to the experimental numbers.

The first observation is that, on the whole, the two simulations agree quite well, although the errors quoted by CP-PACS are in general much smaller. This confirms the previous conclusion that the quenched light hadron spectrum agrees within 10 % with experiment. This independent confirmation, using results in the $O(a)$ improved theory, is an important result, since lattice artefacts for unimproved Wilson fermions are in general much larger [35,9], so that continuum extrapolations can be quite drastic.

It must be mentioned, though, that the overall precision of our results cannot match that of ref. [4] for the following reasons. Firstly, our calculations have been performed in a fairly narrow range of quark masses, for relatively small volumes (mostly for $L \approx 1.5$ fm). Therefore, possible deviations from a linear quark mass dependence close to the chiral limit could not be detected or controlled. This affects mainly states like the ρ , nucleon or the Δ . Indeed, the modelling of the observed downward curvature in the data reported in [4] turned out to be a significant factor in the detection of the deviation from the experimentally observed spectrum. Furthermore, as far as our baryonic data are concerned, the chiral behaviour at $\beta = 5.7$ is not controlled at all, since only two data points have been computed, so that we had to *assume* linearity in the quark mass. Finally, our data are subject to finite-size corrections. For hadron masses computed at the physical values of the quark masses these effects amount to at most 2 % for vector mesons, 1 – 3 % for octet and 4 – 8 % for decuplet baryons (c.f. Tables XV–XVIII).

To some extent one can check against possible finite-size effects in our results by setting the scale using the nucleon mass. As a baryon the nucleon might also be affected more by finite-size effects, and it is reasonable to expect a (partial) cancellation of these effects in the ratios m_{hadron}/m_N . Indeed, as can be seen from Fig. 7 our results in physical units

decrease when the scale is set by m_N rather than m_{K^*} , although the difference is mostly not significant.

If the differences in the results due to different choices of the lattice scale is not attributed to finite-size effects, then they serve to estimate the intrinsic scale ambiguity in the quenched approximation in the continuum limit. On the basis of the results in Tables XV–XVII one can infer that in the most extreme cases the difference between the highest and lowest values in physical units amounts to about 20 %. We may then assign an uncertainty of ± 10 % to our results in physical units as a consequence of the scale ambiguity.

To summarise, we have presented a comprehensive study of the light hadron spectrum in quenched QCD, using improved Wilson actions. Qualitative results indicate an improved behaviour of the pseudoscalar-vector mass splitting. The parameter J , on the other hand, shows no sign of approaching its phenomenological value of 0.48(2), even in the continuum limit. This appears to be an intrinsic feature of the quenched approximation.

Our results show that $O(a)$ improvement works well for spectral quantities. Hadron masses computed for non-perturbative c_{sw} and expressed in units of r_0 show almost no dependence on the lattice spacing for $\beta \geq 6.0$. We also find that the extrapolations to the continuum limit are quite mild in general. That is, for $a \approx 0.1$ fm lattice artefacts amount to about 5 % or less.

We have presented further evidence that the quenched light hadron spectrum agrees with experiment to within 10 %. Further technical improvements, including, in particular, the modelling of the quark mass dependence and the addition of more points in the continuum extrapolations should be implemented to increase the overall precision.

The next step is the extension of this investigation to decay constants and matrix elements. First results have already been presented in [44–46]. Here, an attractive feature is the availability of non-perturbative determinations of some renormalisation factors [47,48].

Acknowledgments. This work was supported by the Particle Physics & Astronomy Research Council (PPARC) through grants GR/L56336 and GR/L29927. We also acknowledge the support by EPSRC under grant GR/K41663. H.P.S. acknowledges the support of the Leverhulme foundation and the JSPS Research for the Future program. HW is grateful to Akira Ukawa for the hospitality at the Center of Computational Physics, University of Tsukuba, where part of this work was completed. DGR and HW acknowledge the support by PPARC through the award of Advanced Fellowships.

REFERENCES

- [1] CP-PACS Collaboration (R. Burkhalter et al.), Nucl. Phys. B (Proc. Suppl.) 73 (1999) 3.
- [2] R.D. Kenway, Nucl. Phys. B (Proc. Suppl.) 73 (1999) 16.
- [3] R. Mawhinney, presented at “Lattice 99”, to appear in the proceedings, hep-lat/0001032.
- [4] CP-PACS Collaboration (S. Aoki et al.), Phys. Rev. Lett 84 (2000) 238.
- [5] F. Butler, H. Chen, J. Sexton, A. Vaccarino and D. Weingarten, Nucl. Phys. B430 (1994) 179.
- [6] C. Bernard et al., Phys. Rev. Lett. 81 (1998) 3087.
- [7] B. Sheikholeslami and R. Wohlert, Nucl. Phys. B259 (1985) 572.
- [8] M. Lüscher, S. Sint, R. Sommer, P. Weisz and U. Wolff, Nucl. Phys. B491 (1997) 323.
- [9] R.G. Edwards, U.M. Heller and T.R. Klassen, Phys. Rev. Lett. 80 (1998) 3448.
- [10] K. Jansen and R. Sommer, Nucl. Phys. B530 (1998) 185.
- [11] G.P. Lepage and P.B. Mackenzie, Phys. Rev. D48 (1993) 2250.
- [12] UKQCD Collaboration (H.P. Shanahan et al.), Phys. Rev. D55 (1997) 1548.
- [13] M. Göckeler et al., Phys. Lett. B391 (1997) 388; Phys. Rev. D57 (1998) 5562.
- [14] S. Collins, R.G. Edwards, U.M. Heller and J. Sloan, Nucl. Phys. B (Proc. Suppl.) 60 (1998) 34.
- [15] A. Cucchieri, M. Masetti, T. Mendes and R. Petronzio, Phys. Lett. B422 (1998) 212; A. Cucchieri, T. Mendes and R. Petronzio, J. High Energy Phys. 05 (1998) 006.
- [16] D. Becirevic et al., hep-lat/9809129.
- [17] ALPHA Collaboration (M. Guagnelli et al.), hep-lat/9903040
- [18] ALPHA and UKQCD Collaborations (J. Garden et al.), hep-lat/9906013.
- [19] UKQCD Collaboration (C.R. Allton et al.), Nucl. Phys. B407 (1993) 331.
- [20] R. Wohlert, Improved continuum limit lattice action for quarks, DESY 87-069, unpublished.
- [21] M. Lüscher and P. Weisz, Nucl. Phys. B479 (1996) 429.
- [22] M. Lüscher, S. Sint, R. Sommer and P. Weisz, Nucl. Phys. B478 (1996) 365.
- [23] S. Sint and P. Weisz, Nucl. Phys. B502 (1997) 251.
- [24] G.M. de Divitiis and R. Petronzio, Phys. Lett. B419 (1998) 311.
- [25] UKQCD Collaboration (P. Lacock et al.), Phys. Rev. D51 (1995) 6403.
- [26] UKQCD Collaboration (C.R. Allton et al.), Phys. Rev. D47 (1993) 5128.
- [27] M. Albanese et al., Phys. Lett. B192 (1987) 163; *ibid.* B197 (1987) 400.
- [28] P.A. Rowland, PhD Thesis, Edinburgh 1997, unpublished.
- [29] UKQCD Collaboration (C.R. Allton et al.), Phys. Rev. D49 (1994) 474.
- [30] K.H. Mütter, Ph. de Forcrand, K. Schilling and R. Sommer, in: Brookhaven 1986, Proceedings, Lattice Gauge Theory 1986, p. 257;
S. Itoh, Y. Iwasaki and T. Yoshié, Phys. Lett. B184 (1987) 375; Phys. Rev. D36 (1987) 527;
Y. Iwasaki, Nucl. Phys. B (Proc. Suppl.) 9 (1989) 254.
- [31] W. Bardeen, A. Duncan, E. Eichten and H. Thacker, Phys. Rev. D59 (1999) 014507;
A. Hoferichter et al., Nucl. Phys. B (Proc. Suppl.) 63 (1998) 164;
M. Göckeler et al., Nucl. Phys. B (Proc. Suppl.) 73 (1999) 889.
- [32] UKQCD Collaboration (M. Teper, H. Simma and D. Smith), Nucl. Phys. B (Proc.

- Suppl.) 63 (1998) 558;
 UKQCD Collaboration (H. Simma and D. Smith), hep-lat/9801025.
- [33] R. Sommer, Nucl. Phys. B411 (1994) 839.
 - [34] M. Guagnelli, R. Sommer and H. Wittig, Nucl. Phys. B535 (1998) 389.
 - [35] H. Wittig, Nucl. Phys. B (Proc. Suppl.) 63 (1998) 47.
 - [36] UKQCD Collaboration (P. Lacock and C. Michael), Phys. Rev. D52 (1995) 5213.
 - [37] J.N. Labrenz and S.R. Sharpe, Phys. Rev. D54 (1996) 4595.
 - [38] T. Bhattacharya, R. Gupta, G. Kilcup and S. Sharpe, Phys. Rev. D53 (1996) 6486.
 - [39] S.R. Sharpe, Phys. Rev. D41 (1990) 3233; *ibid.* D46 (1992) 3146.
 - [40] C.W. Bernard and M.F.L. Golterman, Phys. Rev. D46 (1992) 853.
 - [41] M. Booth, G. Chiladze and A.F. Falk Phys. Rev. D55 (1997) 3092.
 - [42] Review of Particle Physics, (C. Caso et al.), Eur. Phys. J. C3 (1998) 223.
 - [43] ALPHA Collaboration (J. Heitger), Nucl. Phys. B557 (1999) 309.
 - [44] UKQCD Collaboration (R. Kenway), Nucl. Phys. B (Proc. Suppl.) 53 (1997) 206.
 - [45] UKQCD Collaboration (P.A. Rowland), Nucl. Phys. B (Proc. Suppl.) 53 (1997) 308;
 Nucl. Phys. B (Proc. Suppl.) 63 (1998) 173.
 - [46] UKQCD Collaboration (L. Lellouch and C.-J. D. Lin), Nucl. Phys. B (Proc. Suppl.) 73
 (1999) 312.
 - [47] M. Lüscher, S. Sint, R. Sommer and H. Wittig, Nucl. Phys. B491 (1997) 344.
 - [48] ALPHA Collaboration (S. Capitani et al.), Nucl. Phys. B544 (1999) 669.

TABLES

TABLE I. Simulation parameters, statistics and smearing parameters for the NP (upper three rows) and TAD (lower three rows) datasets. Lattice sizes in physical units are estimated using r_0 to set the scale [34]. The number of exceptional configurations removed from the ensemble is denoted in parentheses.

β	c_{sw}	$L^3 \cdot T$	L [fm]	κ	#conf.	smearing
6.0	1.769	$16^3 \cdot 48$	1.5	0.13344, 0.13417, 0.13455	496(3)	fuzz, $r = 6$
		$32^3 \cdot 64$	3.0	0.13344, 0.13417, 0.13455	70(2)	jac, $N_{\text{jac}} = 30$
6.2	1.614	$24^3 \cdot 48$	1.6	0.13460, 0.13510, 0.13530	216	fuzz, $r = 8$
5.7	1.568	$16^3 \cdot 48$	2.7	0.13843, 0.14077	145	jac, $N_{\text{jac}} = 16$
6.0	1.479	$16^3 \cdot 48$	1.5	0.13700, 0.13810, 0.13856	499	fuzz, $r = 6$
6.2	1.442	$24^3 \cdot 48$	1.6	0.13640, 0.13710, 0.13745	218	fuzz, $r = 8$

TABLE II. Pseudoscalar masses for the non-perturbatively improved data sets.

β	$L^3 \cdot T$	κ_1	κ_2	am_{PS}	$[t_{\text{min}}, t_{\text{max}}]$	χ^2 / dof
6.0	$16^3 \cdot 48$	0.13344	0.13344	0.3977^{+13}_{-7}	[6,23]	23.82 / 30
		0.13417	0.13344	0.3553^{+15}_{-7}	[6,23]	24.18 / 30
		0.13455	0.13344	0.3319^{+17}_{-9}	[6,23]	26.70 / 30
		0.13417	0.13417	0.3077^{+18}_{-8}	[6,23]	26.14 / 30
		0.13455	0.13417	0.2805^{+19}_{-10}	[6,23]	27.37 / 30
		0.13455	0.13455	0.2493^{+22}_{-12}	[6,23]	30.84 / 30
6.0	$32^3 \cdot 64$	0.13344	0.13344	0.3952^{+16}_{-8}	[15,31]	14.49 / 15
		0.13417	0.13344	0.3524^{+15}_{-10}	[15,31]	14.86 / 15
		0.13455	0.13344	0.3284^{+15}_{-11}	[15,31]	13.56 / 15
		0.13417	0.13417	0.3048^{+13}_{-11}	[15,31]	13.64 / 15
		0.13455	0.13417	0.2769^{+13}_{-11}	[15,31]	12.22 / 15
		0.13455	0.13455	0.2457^{+14}_{-10}	[15,31]	13.04 / 15
6.2	$24^3 \cdot 48$	0.13460	0.13460	0.2803^{+15}_{-10}	[8,23]	30.99 / 26
		0.13510	0.13460	0.2492^{+17}_{-12}	[8,23]	29.08 / 26
		0.13530	0.13460	0.2361^{+18}_{-14}	[8,23]	28.42 / 26
		0.13510	0.13510	0.2149^{+19}_{-14}	[8,23]	31.54 / 26
		0.13530	0.13510	0.1998^{+19}_{-17}	[8,23]	31.18 / 26
		0.13530	0.13530	0.1836^{+23}_{-18}	[8,23]	32.04 / 26

TABLE III. Vector masses for the non-perturbatively improved data sets.

β	$L^3 \cdot T$	κ_1	κ_2	am_V	$[t_{\min}, t_{\max}]$	χ^2 / dof
6.0	$16^3 \cdot 48$	0.13344	0.13344	0.5397^{+32}_{-30}	[6,23]	24.02 / 30
		0.13417	0.13344	0.5124^{+49}_{-32}	[6,23]	27.16 / 30
		0.13455	0.13344	0.4997^{+51}_{-50}	[6,23]	29.71 / 30
		0.13417	0.13417	0.4852^{+53}_{-53}	[6,23]	27.92 / 30
		0.13455	0.13417	0.4713^{+69}_{-68}	[6,23]	31.96 / 30
		0.13455	0.13455	0.4577^{+85}_{-83}	[6,23]	30.16 / 30
6.0	$32^3 \cdot 64$	0.13344	0.13344	0.5400^{+47}_{-35}	[10,20]	13.68 / 9
		0.13417	0.13344	0.5143^{+53}_{-39}	[10,20]	14.44 / 9
		0.13455	0.13344	0.5019^{+58}_{-46}	[10,20]	13.75 / 9
		0.13417	0.13417	0.4887^{+61}_{-48}	[10,20]	13.30 / 9
		0.13455	0.13417	0.4762^{+74}_{-59}	[10,20]	10.31 / 9
		0.13455	0.13455	0.4636^{+88}_{-76}	[10,20]	6.69 / 9
6.2	$24^3 \cdot 48$	0.13460	0.13460	0.3887^{+32}_{-28}	[8,23]	33.55 / 26
		0.13510	0.13460	0.3708^{+42}_{-36}	[8,23]	28.99 / 26
		0.13530	0.13460	0.3645^{+43}_{-47}	[8,23]	26.51 / 26
		0.13510	0.13510	0.3531^{+55}_{-51}	[8,23]	29.56 / 26
		0.13530	0.13510	0.3471^{+62}_{-61}	[8,23]	27.91 / 26
		0.13530	0.13530	0.3414^{+72}_{-82}	[8,23]	30.98 / 26

TABLE IV. Pseudoscalar masses for the tadpole improved data sets.

β	$L^3 \cdot T$	κ_1	κ_2	am_{PS}	$[t_{\min}, t_{\max}]$	χ^2 / dof
5.7	$16^3 \cdot 32$	0.13843	0.13843	0.7350^{+11}_{-6}	[6,15]	23.99 / 14
		0.14077	0.13843	0.6404^{+11}_{-29}	[5,15]	16.89 / 16
		0.14077	0.14077	0.5307^{+19}_{-20}	[5,15]	16.00 / 16
6.0	$16^3 \cdot 48$	0.13700	0.13700	0.4131^{+13}_{-7}	[6,23]	22.57 / 30
		0.13810	0.13700	0.3572^{+16}_{-6}	[6,23]	21.97 / 30
		0.13856	0.13700	0.3320^{+21}_{-6}	[6,23]	27.82 / 30
		0.13810	0.13810	0.2927^{+21}_{-4}	[6,23]	26.93 / 30
		0.13856	0.13810	0.2621^{+23}_{-7}	[6,23]	29.93 / 30
		0.13856	0.13856	0.2268^{+25}_{-10}	[6,23]	30.40 / 30
6.2	$24^3 \cdot 48$	0.13640	0.13640	0.3033^{+12}_{-10}	[8,23]	30.03 / 26
		0.13710	0.13640	0.2643^{+15}_{-11}	[8,23]	29.29 / 26
		0.13745	0.13640	0.2436^{+18}_{-13}	[8,23]	29.02 / 26
		0.13710	0.13710	0.2206^{+18}_{-12}	[8,23]	31.97 / 26
		0.13745	0.13710	0.1959^{+21}_{-16}	[8,23]	30.92 / 26
		0.13745	0.13745	0.1680^{+27}_{-18}	[8,23]	31.13 / 26

TABLE V. Vector masses for the tadpole improved data sets.

β	$L^3 \cdot T$	κ_1	κ_2	am_V	$[t_{\min}, t_{\max}]$	χ^2/dof
5.7	$16^3 \cdot 32$	0.13843	0.13843	0.9332^{+45}_{-37}	[7,15]	12.80 / 12
		0.14077	0.13843	0.8688^{+54}_{-48}	[7,15]	11.96 / 12
		0.14077	0.14077	0.809^{+9}_{-13}	[7,15]	10.76 / 12
6.0	$16^3 \cdot 48$	0.13700	0.13700	0.5386^{+32}_{-22}	[7,23]	23.82 / 28
		0.13810	0.13700	0.5030^{+40}_{-24}	[6,23]	27.20 / 30
		0.13856	0.13700	0.4889^{+45}_{-41}	[6,23]	27.83 / 30
		0.13810	0.13810	0.4652^{+52}_{-44}	[6,23]	26.92 / 30
		0.13856	0.13810	0.4501^{+66}_{-62}	[6,23]	29.23 / 30
		0.13856	0.13856	0.4353^{+88}_{-76}	[6,23]	25.43 / 30
6.2	$24^3 \cdot 48$	0.13640	0.13640	0.4005^{+23}_{-26}	[8,23]	32.65 / 26
		0.13710	0.13640	0.3761^{+34}_{-29}	[8,23]	28.79 / 26
		0.13745	0.13640	0.3648^{+39}_{-44}	[8,23]	25.39 / 26
		0.13710	0.13710	0.3522^{+50}_{-44}	[8,23]	26.83 / 26
		0.13745	0.13710	0.3412^{+64}_{-63}	[8,23]	24.85 / 26
		0.13745	0.13745	0.3306^{+90}_{-95}	[8,23]	28.83 / 26

TABLE VI. Masses for the nucleon and Δ for degenerate quark mass combinations for the non-perturbatively improved data.

β	$L^3 \cdot T$	κ	am_N	$[t_{\min}, t_{\max}]$	χ^2/dof	am_Δ	$[t_{\min}, t_{\max}]$	χ^2/dof
6.0	$16^3 \cdot 48$	0.13344	0.808^{+10}_{-7}	[9,23]	25.42/24	0.913^{+9}_{-22}	[9,23]	21.84/24
		0.13417	0.711^{+16}_{-13}	[9,23]	25.74/24	0.852^{+19}_{-23}	[9,23]	31.33/24
		0.13455	0.665^{+26}_{-28}	[9,23]	26.98/24	0.768^{+52}_{-36}	[10,23]	40.37/22
6.0	$32^3 \cdot 64$	0.13344	0.799^{+10}_{-10}	[3,18]	16.82/12	0.899^{+13}_{-14}	[2,16]	17.56/11
		0.13417	0.700^{+11}_{-15}	[3,18]	15.99/12	0.818^{+16}_{-13}	[2,16]	20.09/11
		0.13455	0.641^{+16}_{-20}	[3,18]	14.63/12	0.781^{+18}_{-14}	[2,16]	21.66/11
6.2	$24^3 \cdot 48$	0.13460	0.586^{+8}_{-6}	[10,23]	42.46/22	0.671^{+8}_{-7}	[11,23]	20.35/20
		0.13510	0.509^{+10}_{-10}	[10,23]	41.09/22	0.618^{+14}_{-12}	[11,23]	21.54/20
		0.13530	0.487^{+3}_{-14}	[10,23]	30.35/22	0.596^{+19}_{-13}	[11,23]	20.31/20

TABLE VII. Masses for the nucleon and Δ for degenerate quark mass combinations for the tadpole improved data.

β	$L^3 \cdot T$	κ	am_N	$[t_{\min}, t_{\max}]$	χ^2/dof	am_Δ	$[t_{\min}, t_{\max}]$	χ^2/dof
5.7	$16^3 \cdot 32$	0.13843	1.423^{+12}_{-4}	[7,15]	7.37/12	1.539^{+21}_{-8}	[7,15]	23.62/12
		0.14077	1.183^{+14}_{-11}	[6,15]	15.96/14	1.334^{+26}_{-17}	[7,15]	10.59/12
6.0	$16^3 \cdot 48$	0.13700	0.817^{+9}_{-4}	[10,23]	21.26/22	0.909^{+7}_{-9}	[10,23]	23.49/22
		0.13810	0.678^{+17}_{-8}	[10,23]	27.46/22	0.810^{+13}_{-13}	[8,23]	23.95/26
		0.13856	0.616^{+26}_{-16}	[10,23]	26.95/22	0.774^{+21}_{-26}	[8,23]	41.53/26
6.2	$24^3 \cdot 48$	0.13640	0.608^{+8}_{-6}	[11,23]	34.87/20	0.691^{+7}_{-7}	[11,23]	19.42/20
		0.13710	0.509^{+12}_{-9}	[11,23]	38.62/20	0.620^{+11}_{-10}	[11,23]	23.87/20
		0.13745	0.467^{+12}_{-20}	[11,23]	22.68/20	0.577^{+19}_{-13}	[11,23]	20.60/20

TABLE VIII. Masses for Σ -like, Λ -like and Δ -like baryons for non-degenerate quark masses for $\beta = 6.0$, $L^3 \cdot T = 16^3 \cdot 48$ for the non-perturbatively improved data.

κ_1	κ_2	κ_3	am_Σ	am_Λ	am_Δ
0.13344	0.13344	0.13417	0.780^{+10}_{-6}	0.775^{+11}_{-6}	0.894^{+11}_{-12}
0.13344	0.13344	0.13455	0.766^{+11}_{-7}	0.757^{+12}_{-7}	0.890^{+14}_{-12}
0.13344	0.13417	0.13417	0.743^{+12}_{-8}	0.744^{+13}_{-7}	0.872^{+14}_{-13}
0.13344	0.13417	0.13455	0.735^{+12}_{-10}	0.722^{+15}_{-10}	0.871^{+15}_{-14}
0.13344	0.13455	0.13455	0.708^{+13}_{-14}	0.713^{+16}_{-11}	0.860^{+19}_{-18}
0.13417	0.13344	0.13344	0.771^{+11}_{-6}	0.781^{+11}_{-6}	
0.13417	0.13344	0.13417	0.745^{+14}_{-7}	0.739^{+12}_{-8}	
0.13417	0.13344	0.13455	0.728^{+12}_{-10}	0.727^{+14}_{-9}	
0.13417	0.13417	0.13455	0.697^{+13}_{-13}	0.692^{+16}_{-12}	0.845^{+21}_{-20}
0.13417	0.13455	0.13455	0.677^{+15}_{-17}	0.679^{+17}_{-15}	0.837^{+25}_{-27}
0.13455	0.13344	0.13344	0.750^{+13}_{-7}	0.769^{+12}_{-8}	
0.13455	0.13344	0.13417	0.719^{+15}_{-10}	0.734^{+13}_{-10}	
0.13455	0.13344	0.13455	0.717^{+15}_{-12}	0.702^{+14}_{-14}	
0.13455	0.13417	0.13417	0.689^{+18}_{-13}	0.698^{+14}_{-13}	
0.13455	0.13417	0.13455	0.679^{+18}_{-15}	0.674^{+15}_{-19}	

TABLE IX. Masses for Σ -like, Λ -like and Δ -like baryons for non-degenerate quark masses for $\beta = 6.0$, $L^3 \cdot T = 32^3 \cdot 64$ for the non-perturbatively improved data.

κ_1	κ_2	κ_3	am_Σ	am_Λ	am_Δ
0.13344	0.13344	0.13417	0.769^{+10}_{-11}	0.765^{+10}_{-11}	0.873^{+14}_{-14}
0.13344	0.13344	0.13455	0.755^{+10}_{-12}	0.748^{+10}_{-13}	0.859^{+15}_{-13}
0.13344	0.13417	0.13417	0.732^{+10}_{-13}	0.737^{+10}_{-12}	0.845^{+15}_{-14}
0.13344	0.13417	0.13455	0.726^{+10}_{-13}	0.711^{+10}_{-15}	0.832^{+16}_{-13}
0.13344	0.13455	0.13455	0.695^{+12}_{-16}	0.704^{+10}_{-15}	0.820^{+17}_{-13}
0.13417	0.13344	0.13344	0.764^{+9}_{-11}	0.772^{+10}_{-11}	
0.13417	0.13344	0.13417	0.740^{+10}_{-12}	0.730^{+10}_{-13}	
0.13417	0.13344	0.13455	0.716^{+10}_{-14}	0.719^{+11}_{-14}	
0.13417	0.13417	0.13455	0.684^{+12}_{-16}	0.680^{+12}_{-16}	0.805^{+17}_{-13}
0.13417	0.13455	0.13455	0.659^{+15}_{-19}	0.664^{+13}_{-18}	0.793^{+18}_{-14}
0.13455	0.13344	0.13344	0.745^{+10}_{-13}	0.759^{+10}_{-11}	
0.13455	0.13344	0.13417	0.712^{+11}_{-14}	0.724^{+10}_{-14}	
0.13455	0.13344	0.13455	0.711^{+10}_{-15}	0.691^{+12}_{-16}	
0.13455	0.13417	0.13417	0.678^{+13}_{-16}	0.684^{+10}_{-17}	
0.13455	0.13417	0.13455	0.666^{+13}_{-18}	0.657^{+16}_{-19}	

TABLE X. Masses for Σ -like, Λ -like and Δ -like baryons for non-degenerate quark masses for $\beta = 6.2$, $L^3 \cdot T = 24^3 \cdot 48$ for the non-perturbatively improved data.

κ_1	κ_2	κ_3	am_Σ	am_Λ	am_Δ
0.13460	0.13460	0.13510	0.555^{+3}_{-9}	0.548^{+8}_{-7}	0.656^{+7}_{-8}
0.13460	0.13460	0.13530	0.547^{+1}_{-10}	0.534^{+9}_{-8}	0.648^{+8}_{-8}
0.13460	0.13510	0.13510	0.528^{+8}_{-10}	0.524^{+9}_{-8}	0.638^{+9}_{-8}
0.13460	0.13510	0.13530	0.522^{+10}_{-10}	0.510^{+7}_{-11}	0.630^{+10}_{-8}
0.13460	0.13530	0.13530	0.513^{+7}_{-12}	0.502^{+8}_{-12}	0.623^{+11}_{-9}
0.13510	0.13460	0.13460	0.545^{+9}_{-6}	0.552^{+9}_{-7}	
0.13510	0.13460	0.13510	0.525^{+9}_{-8}	0.522^{+9}_{-10}	
0.13510	0.13460	0.13530	0.514^{+9}_{-10}	0.516^{+7}_{-10}	
0.13510	0.13510	0.13530	0.500^{+6}_{-11}	0.497^{+3}_{-11}	0.611^{+12}_{-10}
0.13510	0.13530	0.13530	0.497^{+7}_{-11}	0.474^{+4}_{-27}	0.606^{+13}_{-11}
0.13530	0.13460	0.13460	0.530^{+9}_{-7}	0.543^{+10}_{-7}	
0.13530	0.13460	0.13510	0.509^{+7}_{-11}	0.516^{+11}_{-10}	
0.13530	0.13460	0.13530	0.503^{+9}_{-11}	0.507^{+6}_{-14}	
0.13530	0.13510	0.13510	0.493^{+1}_{-12}	0.497^{+7}_{-13}	
0.13530	0.13510	0.13530	0.487^{+1}_{-13}	0.497^{+4}_{-15}	

TABLE XI. Masses for Σ -like, Λ -like and Δ -like baryons for non-degenerate quark masses for $\beta = 6.0$, $L^3 \cdot T = 16^3 \cdot 48$ for the tadpole improved data.

κ_1	κ_2	κ_3	am_Σ	am_Λ	am_Δ
0.13700	0.13700	0.13810	0.777^{+11}_{-5}	0.771^{+11}_{-5}	0.873^{+8}_{-9}
0.13700	0.13700	0.13856	0.761^{+12}_{-5}	0.749^{+13}_{-6}	0.882^{+6}_{-15}
0.13700	0.13810	0.13810	0.722^{+14}_{-7}	0.732^{+13}_{-7}	0.853^{+4}_{-18}
0.13700	0.13810	0.13856	0.713^{+15}_{-8}	0.703^{+16}_{-9}	0.845^{+9}_{-17}
0.13700	0.13856	0.13856	0.678^{+19}_{-12}	0.697^{+15}_{-9}	0.832^{+12}_{-17}
0.13810	0.13700	0.13700	0.766^{+11}_{-5}	0.778^{+12}_{-5}	
0.13810	0.13700	0.13810	0.733^{+14}_{-7}	0.718^{+14}_{-7}	
0.13810	0.13700	0.13856	0.706^{+14}_{-7}	0.707^{+15}_{-8}	
0.13810	0.13810	0.13856	0.659^{+18}_{-13}	0.659^{+20}_{-12}	0.810^{+12}_{-20}
0.13810	0.13856	0.13856	0.634^{+22}_{-19}	0.643^{+20}_{-12}	0.787^{+19}_{-19}
0.13856	0.13700	0.13700	0.741^{+13}_{-7}	0.763^{+14}_{-5}	
0.13856	0.13700	0.13810	0.698^{+17}_{-8}	0.710^{+16}_{-7}	
0.13856	0.13700	0.13856	0.697^{+15}_{-8}	0.672^{+18}_{-12}	
0.13856	0.13810	0.13810	0.654^{+21}_{-11}	0.655^{+18}_{-12}	
0.13856	0.13810	0.13856	0.642^{+21}_{-10}	0.626^{+23}_{-19}	

TABLE XII. Masses for Σ -like, Λ -like and Δ -like baryons for non-degenerate quark masses for $\beta = 6.2$, $L^3 \cdot T = 24^3 \cdot 48$ for the tadpole improved data.

κ_1	κ_2	κ_3	am_Σ	am_Λ	am_Δ
0.13640	0.13640	0.13710	0.576^{+3}_{-8}	0.568^{+7}_{-6}	0.656^{+7}_{-6}
0.13640	0.13640	0.13745	0.554^{+6}_{-7}	0.545^{+9}_{-7}	0.652^{+8}_{-7}
0.13640	0.13710	0.13710	0.539^{+9}_{-8}	0.535^{+11}_{-7}	0.642^{+9}_{-7}
0.13640	0.13710	0.13745	0.526^{+9}_{-8}	0.510^{+9}_{-9}	0.627^{+10}_{-8}
0.13640	0.13745	0.13745	0.504^{+9}_{-13}	0.491^{+16}_{-10}	0.619^{+11}_{-9}
0.13710	0.13640	0.13640	0.563^{+6}_{-5}	0.571^{+8}_{-7}	
0.13710	0.13640	0.13710	0.539^{+7}_{-8}	0.532^{+11}_{-8}	
0.13710	0.13640	0.13745	0.515^{+10}_{-8}	0.518^{+8}_{-8}	
0.13710	0.13710	0.13745	0.494^{+6}_{-11}	0.491^{+3}_{-11}	0.602^{+11}_{-10}
0.13710	0.13745	0.13745	0.463^{+12}_{-24}	0.457^{+5}_{-22}	0.593^{+12}_{-11}
0.13745	0.13640	0.13640	0.540^{+6}_{-7}	0.558^{+9}_{-7}	
0.13745	0.13640	0.13710	0.510^{+10}_{-8}	0.522^{+10}_{-9}	
0.13745	0.13640	0.13745	0.497^{+15}_{-9}	0.492^{+8}_{-15}	
0.13745	0.13710	0.13710	0.470^{+8}_{-19}	0.492^{+7}_{-13}	
0.13745	0.13710	0.13745	0.455^{+7}_{-23}	0.451^{+13}_{-25}	

TABLE XIII. Values for κ_c for all datasets. The labels ‘tree’, ‘bare’ and ‘tad’ refer to the coefficient b_m estimated either at tree-level, bare and tadpole improved one-loop perturbation theory, respectively. Also shown are the results of ref. [8], obtained using the current quark mass instead of the pseudoscalar mass.

	β	$L^3 \cdot T$	$b_m = 0$	tree	bare	tad	ref. [8]
NP	6.0	$16^3 \cdot 48$		0.135259^{+16}_{-9}	0.135255^{+16}_{-9}	0.135252^{+16}_{-9}	0.135196(14)
	6.0	$32^3 \cdot 64$		0.135241^{+9}_{-10}	0.135237^{+9}_{-10}	0.135235^{+9}_{-10}	
	6.2	$24^3 \cdot 48$		0.135818^{+17}_{-14}	0.135816^{+17}_{-14}	0.135815^{+17}_{-14}	0.135795(13)
TAD	5.7	$16^3 \cdot 48$	0.143408^{+29}_{-45}	0.143240^{+27}_{-40}	0.143206^{+26}_{-39}	0.143179^{+26}_{-38}	
	6.0	$16^3 \cdot 48$	0.139240^{+20}_{-7}	0.139216^{+19}_{-6}	0.139212^{+19}_{-6}	0.139209^{+19}_{-6}	
	6.2	$24^3 \cdot 48$	0.137912^{+19}_{-13}	0.137900^{+18}_{-12}	0.137898^{+18}_{-12}	0.137897^{+18}_{-12}	

TABLE XIV. Values for κ_n and κ_s determined for three different quantities Q to set the lattice scale. All estimates were obtained by setting b_m equal to its tadpole improved perturbative value.

	β	$L^3 \cdot T$	$Q = r_0^{-1}$		$Q = m_{K^*}$		$Q = m_N$	
			κ_n	κ_s	κ_n	κ_s	κ_n	κ_s
NP	6.0	$16^3 \cdot 48$	0.13520^{+1}_{-2}	0.13401^{+2}_{-2}	0.13520^{+2}_{-1}	0.13383^{+4}_{-6}	0.13517^{+2}_{-2}	0.13318^{+19}_{-18}
	6.0	$32^3 \cdot 64$	0.13519^{+1}_{-1}	0.13398^{+2}_{-2}	0.13518^{+1}_{-1}	0.13376^{+5}_{-7}	0.13516^{+1}_{-1}	0.13327^{+19}_{-14}
	6.2	$24^3 \cdot 48$	0.13578^{+1}_{-2}	0.13495^{+2}_{-2}	0.13577^{+2}_{-1}	0.13476^{+3}_{-5}	0.13576^{+2}_{-1}	0.13438^{+13}_{-4}
TAD	5.7	$16^3 \cdot 48$	0.14306^{+4}_{-3}	0.14012^{+5}_{-3}	0.14307^{+3}_{-4}	0.14029^{+11}_{-10}	0.14302^{+3}_{-4}	0.13904^{+22}_{-21}
	6.0	$16^3 \cdot 48$	0.13915^{+1}_{-2}	0.13780^{+1}_{-2}	0.13915^{+2}_{-1}	0.13769^{+5}_{-5}	0.13913^{+2}_{-1}	0.13712^{+13}_{-20}
	6.2	$24^3 \cdot 48$	0.13786^{+1}_{-2}	0.13699^{+2}_{-2}	0.13785^{+2}_{-1}	0.13680^{+3}_{-5}	0.13784^{+2}_{-1}	0.13655^{+12}_{-6}

TABLE XV. Results for the physical meson and baryon masses with the lattice scale set by r_0 .

β	$m_\rho r_0$		$m_{K^*} r_0$		$m_\phi r_0$	
	NP	TAD	NP	TAD	NP	TAD
5.7		1.982^{+38}_{-54}		2.224^{+28}_{-39}		2.466^{+19}_{-25}
6.0	2.189^{+56}_{-56}	2.121^{+48}_{-49}	2.422^{+41}_{-42}	2.356^{+36}_{-36}	2.655^{+29}_{-28}	2.592^{+25}_{-23}
6.2	2.254^{+69}_{-81}	2.211^{+66}_{-67}	2.468^{+51}_{-55}	2.433^{+48}_{-50}	2.682^{+34}_{-35}	2.654^{+33}_{-34}
Cont.	2.352(163)		2.540(117)		2.729(77)	

β	$m_N r_0$		$m_\Sigma r_0$		$m_\Lambda r_0$		$m_\Xi r_0$	
	NP	TAD	NP	TAD	NP	TAD	NP	TAD
5.7		2.74^{+6}_{-7}		3.05^{+5}_{-5}		3.05^{+5}_{-5}		3.35^{+5}_{-4}
6.0	3.08^{+13}_{-13}	2.92^{+14}_{-9}	3.36^{+10}_{-11}	3.22^{+11}_{-7}	3.34^{+11}_{-11}	3.21^{+11}_{-7}	3.63^{+9}_{-8}	3.52^{+9}_{-5}
6.2	3.02^{+4}_{-14}	2.87^{+6}_{-12}	3.31^{+4}_{-11}	3.18^{+5}_{-9}	3.30^{+3}_{-12}	3.18^{+4}_{-10}	3.59^{+3}_{-8}	3.50^{+4}_{-7}
Cont.	2.92(24)		3.23(19)		3.22(20)		3.54(15)	

β	$m_\Delta r_0$		$m_{\Sigma^*} r_0$		$m_{\Xi^*} r_0$		$m_\Omega r_0$	
	NP	TAD	NP	TAD	NP	TAD	NP	TAD
5.7		3.29^{+12}_{-9}		3.55^{+10}_{-7}		3.81^{+8}_{-6}		4.08^{+7}_{-4}
6.0	4.12^{+26}_{-19}	3.93^{+11}_{-16}	4.29^{+20}_{-16}	4.13^{+9}_{-13}	4.47^{+14}_{-12}	4.32^{+6}_{-10}	4.64^{+9}_{-9}	4.52^{+5}_{-8}
6.2	4.02^{+16}_{-12}	3.96^{+11}_{-9}	4.24^{+13}_{-10}	4.18^{+9}_{-7}	4.46^{+10}_{-8}	4.40^{+7}_{-6}	4.68^{+7}_{-6}	4.62^{+6}_{-5}
Cont.	3.86(37)		4.15(29)		4.44(22)		4.72(17)	

 TABLE XVI. Same as Table XV but with the scale set by m_{K^*} .

β	m_ρ/m_{K^*}		m_ϕ/m_{K^*}	
	NP	TAD	NP	TAD
5.7		0.896^{+3}_{-9}		1.105^{+2}_{-4}
6.0	0.890^{+10}_{-17}	0.887^{+10}_{-13}	1.113^{+1}_{-7}	1.107^{+4}_{-6}
6.2	0.903^{+12}_{-25}	0.893^{+14}_{-23}	1.112^{+2}_{-10}	1.107^{+2}_{-10}
Cont.	0.921^{+32}_{-56}		1.110^{+8}_{-21}	

β	m_N/m_{K^*}		m_Σ/m_{K^*}		m_Λ/m_{K^*}		m_Ξ/m_{K^*}	
	NP	TAD	NP	TAD	NP	TAD	NP	TAD
5.7		1.239^{+37}_{-37}		1.372^{+32}_{-29}		1.372^{+32}_{-29}		1.504^{+28}_{-22}
6.0	1.253^{+51}_{-64}	1.220^{+57}_{-41}	1.385^{+41}_{-50}	1.360^{+46}_{-32}	1.379^{+40}_{-50}	1.356^{+45}_{-31}	1.517^{+31}_{-35}	1.500^{+36}_{-24}
6.2	1.212^{+18}_{-68}	1.160^{+22}_{-56}	1.352^{+15}_{-52}	1.312^{+18}_{-43}	1.347^{+13}_{-55}	1.313^{+13}_{-44}	1.491^{+14}_{-37}	1.465^{+13}_{-33}
Cont.	1.14^{+6}_{-18}		1.29^{+5}_{-14}		1.29^{+5}_{-15}		1.45^{+4}_{-10}	

β	m_Δ/m_{K^*}		m_{Σ^*}/m_{K^*}		m_{Ξ^*}/m_{K^*}		m_Ω/m_{K^*}	
	NP	TAD	NP	TAD	NP	TAD	NP	TAD
5.7		1.487^{+55}_{-46}		1.600^{+49}_{-36}		1.713^{+43}_{-28}		1.826^{+36}_{-21}
6.0	1.672^{+99}_{-88}	1.645^{+44}_{-71}	1.756^{+70}_{-67}	1.735^{+34}_{-60}	1.841^{+46}_{-52}	1.825^{+26}_{-47}	1.926^{+26}_{-40}	1.916^{+20}_{-37}
6.2	1.609^{+59}_{-58}	1.598^{+42}_{-47}	1.716^{+43}_{-50}	1.705^{+32}_{-38}	1.823^{+31}_{-41}	1.811^{+24}_{-32}	1.930^{+22}_{-36}	1.918^{+20}_{-30}
Cont.	1.50^{+17}_{-17}		1.64^{+13}_{-13}		1.79^{+9}_{-10}		1.93^{+7}_{-8}	

TABLE XVII. Same as Table XV but with the scale set by the nucleon mass m_N .

m_ρ/m_N			m_{K^*}/m_N		m_ϕ/m_N			
β	NP	TAD	NP	TAD	NP	TAD		
5.7		0.727^{+25}_{-30}		0.843^{+18}_{-20}		0.959^{+13}_{-12}		
6.0	0.709^{+37}_{-34}	0.726^{+27}_{-36}	0.837^{+28}_{-24}	0.848^{+20}_{-27}	0.965^{+21}_{-17}	0.970^{+15}_{-20}		
6.2	0.744^{+44}_{-23}	0.769^{+39}_{-21}	0.859^{+34}_{-14}	0.882^{+31}_{-15}	0.975^{+26}_{-7}	0.995^{+24}_{-12}		
Cont.		0.796^{+86}_{-48}		0.894^{+65}_{-29}		0.992^{+51}_{-22}		
m_Σ/m_N			m_Λ/m_N		m_Ξ/m_N			
β	NP	TAD	NP	TAD	NP	TAD		
5.7		1.150^{+5}_{-3}		1.150^{+5}_{-3}		1.299^{+9}_{-5}		
6.0	1.151^{+10}_{-8}	1.156^{+6}_{-7}	1.148^{+10}_{-9}	1.153^{+7}_{-9}	1.303^{+20}_{-16}	1.311^{+11}_{-13}		
6.2	1.154^{+12}_{-6}	1.162^{+8}_{-5}	1.151^{+11}_{-9}	1.162^{+10}_{-10}	1.308^{+23}_{-12}	1.323^{+16}_{-9}		
Cont.		1.161^{+23}_{-12}		1.157^{+21}_{-20}		1.321^{+46}_{-25}		
m_Δ/m_N			m_{Σ^*}/m_N		m_{Ξ^*}/m_N		m_Ω/m_N	
β	NP	TAD	NP	TAD	NP	TAD	NP	TAD
5.7		1.198^{+49}_{-40}		1.326^{+42}_{-30}		1.454^{+35}_{-23}		1.582^{+31}_{-16}
6.0	1.330^{+99}_{-75}	1.344^{+47}_{-83}	1.427^{+76}_{-60}	1.445^{+37}_{-70}	1.524^{+53}_{-51}	1.545^{+28}_{-57}	1.621^{+49}_{-57}	1.646^{+28}_{-49}
6.2	1.325^{+94}_{-36}	1.376^{+78}_{-35}	1.443^{+76}_{-30}	1.488^{+65}_{-28}	1.561^{+60}_{-23}	1.601^{+57}_{-25}	1.679^{+49}_{-24}	1.714^{+50}_{-23}
Cont.		1.33^{+20}_{-10}		1.47^{+16}_{-7}		1.61^{+12}_{-5}		1.76^{+10}_{-4}

 TABLE XVIII. Results for the physical meson and baryons masses at $\beta = 6.0$ on $32^3 \cdot 64$.

	m_ρ/Q	m_{K^*}/Q	m_ϕ/Q	
$Q = r_0^{-1}$	2.243^{+59}_{-51}	2.461^{+45}_{-38}	2.680^{+32}_{-27}	
$Q = m_{K^*}$	0.898^{+13}_{-12}		1.111^{+5}_{-7}	
$Q = m_N$	0.746^{+42}_{-27}	0.863^{+34}_{-21}	0.980^{+28}_{-17}	
	m_N/Q	m_Σ/Q	m_Λ/Q	m_Ξ/Q
$Q = r_0^{-1}$	3.00^{+10}_{-15}	3.29^{+8}_{-11}	3.27^{+8}_{-12}	3.58^{+7}_{-9}
$Q = m_{K^*}$	1.201^{+43}_{-62}	1.343^{+32}_{-51}	1.337^{+32}_{-52}	1.484^{+25}_{-38}
$Q = m_N$		1.155^{+9}_{-9}	1.151^{+8}_{-9}	1.310^{+18}_{-18}
	m_Δ/Q	m_{Σ^*}/Q	m_{Ξ^*}/Q	m_Ω/Q
$Q = r_0^{-1}$	3.81^{+14}_{-10}	4.03^{+12}_{-8}	4.26^{+10}_{-8}	4.48^{+8}_{-7}
$Q = m_{K^*}$	1.525^{+58}_{-46}	1.635^{+46}_{-41}	1.745^{+38}_{-37}	1.855^{+32}_{-37}
$Q = m_N$	1.267^{+73}_{-43}	1.387^{+63}_{-37}	1.508^{+53}_{-33}	1.628^{+46}_{-34}

TABLE XIX. Results for vector mesons, octet (Σ -like) and decuplet (Δ -like) baryons, in units of r_0 , interpolated to the reference points defined by $(m_{\text{PS}}r_0)^2 = 3.0$ and $m_{\text{PS}}/m_V = 0.7$.

$(m_{\text{PS}}r_0)^2 = 3.0$						
	$m_V r_0$		$m_\Sigma r_0$		$m_\Delta r_0$	
β	NP	TAD	NP	TAD	NP	TAD
5.7		2.466^{+23}_{-31}		3.651^{+39}_{-28}		4.067^{+69}_{-40}
6.0	2.649^{+29}_{-29}	2.586^{+25}_{-23}	3.897^{+67}_{-54}	3.805^{+70}_{-41}	4.638^{+89}_{-93}	4.508^{+44}_{-79}
6.2	2.677^{+34}_{-35}	2.649^{+33}_{-34}	3.871^{+36}_{-63}	3.806^{+36}_{-56}	4.668^{+70}_{-65}	4.612^{+57}_{-49}
Cont.	2.725(78)		3.83(12)		4.71(17)	
$m_{\text{PS}}/m_V = 0.7$						
	$m_V r_0$		$m_\Sigma r_0$		$m_\Delta r_0$	
β	NP	TAD	NP	TAD	NP	TAD
5.7		2.451^{+32}_{-35}		3.633^{+49}_{-41}		4.051^{+79}_{-55}
6.0	2.760^{+37}_{-35}	2.669^{+37}_{-25}	4.112^{+68}_{-48}	3.957^{+75}_{-37}	4.776^{+64}_{-80}	4.607^{+46}_{-69}
6.2	2.796^{+45}_{-39}	2.758^{+43}_{-36}	4.115^{+63}_{-66}	4.043^{+53}_{-56}	4.855^{+63}_{-68}	4.777^{+62}_{-52}
Cont.	2.845(94)		4.13(15)		4.97(15)	

FIGURES

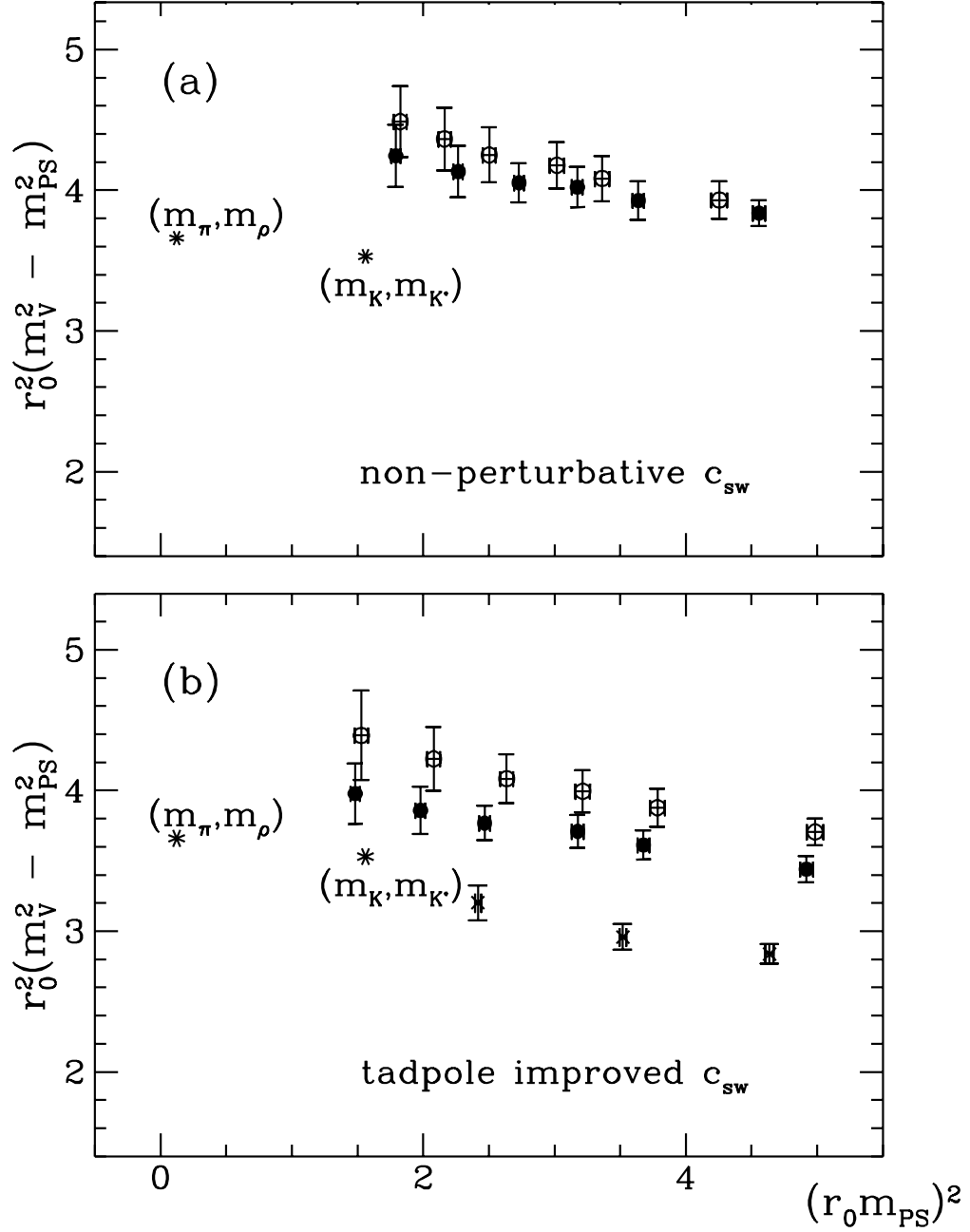


FIG. 1. The vector-pseudoscalar hyperfine splittings for (a): the NP and (b): the TAD datasets. Open squares, full circles and crosses denote the data at $\beta = 6.2$, 6.0 and 5.7 , respectively. The experimental points are represented by the asterisks.

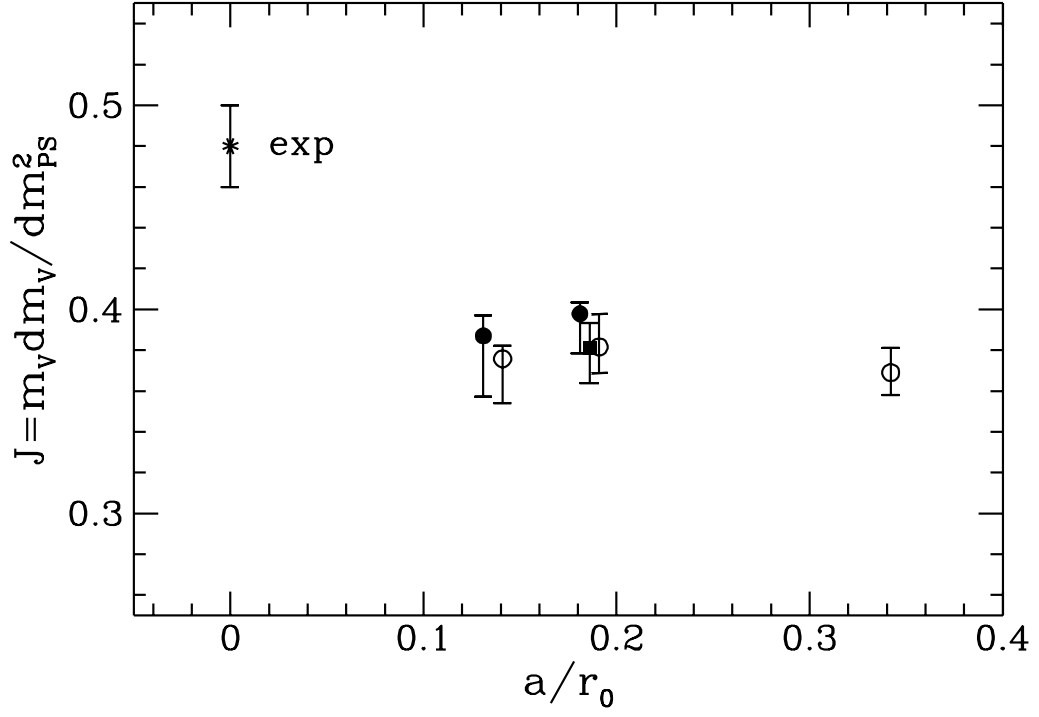


FIG. 2. The parameter J plotted versus the lattice spacing in units of r_0 . Filled (open) symbols denote the data using non-perturbative (tadpole improved) c_{sw} . The filled square denotes the data point at $\beta = 6.0$ on the larger volume of $32^3 \cdot 64$.

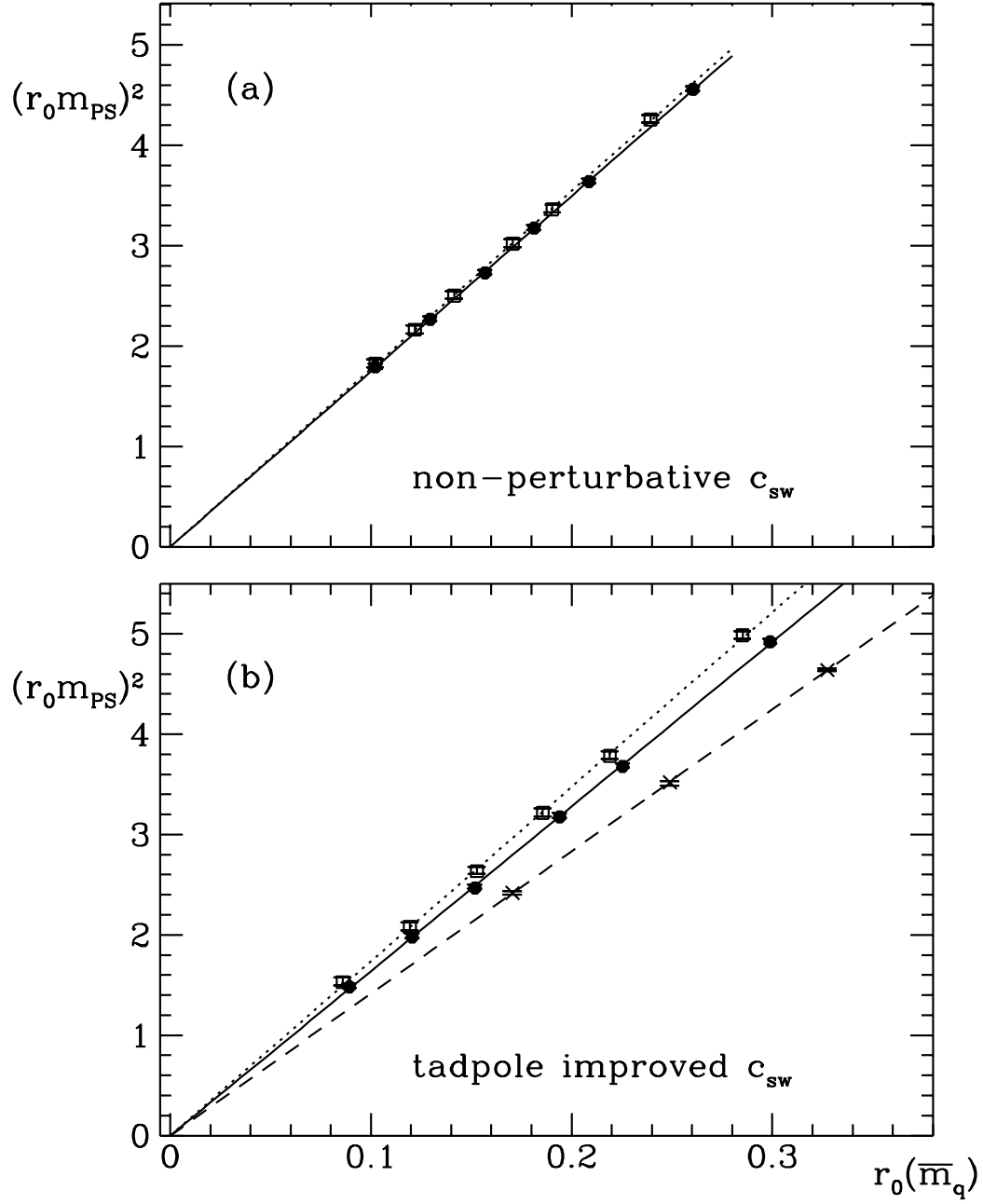


FIG. 3. The pseudoscalar squared plotted versus the averaged quark mass, $\overline{m}_q = (\tilde{m}_{q,1} + \tilde{m}_{q,2})/2$ in units of r_0 for (a): the NP and (b): the TAD datasets. Open squares, full circles and crosses denote the data at $\beta = 6.2$, 6.0 and 5.7, respectively.

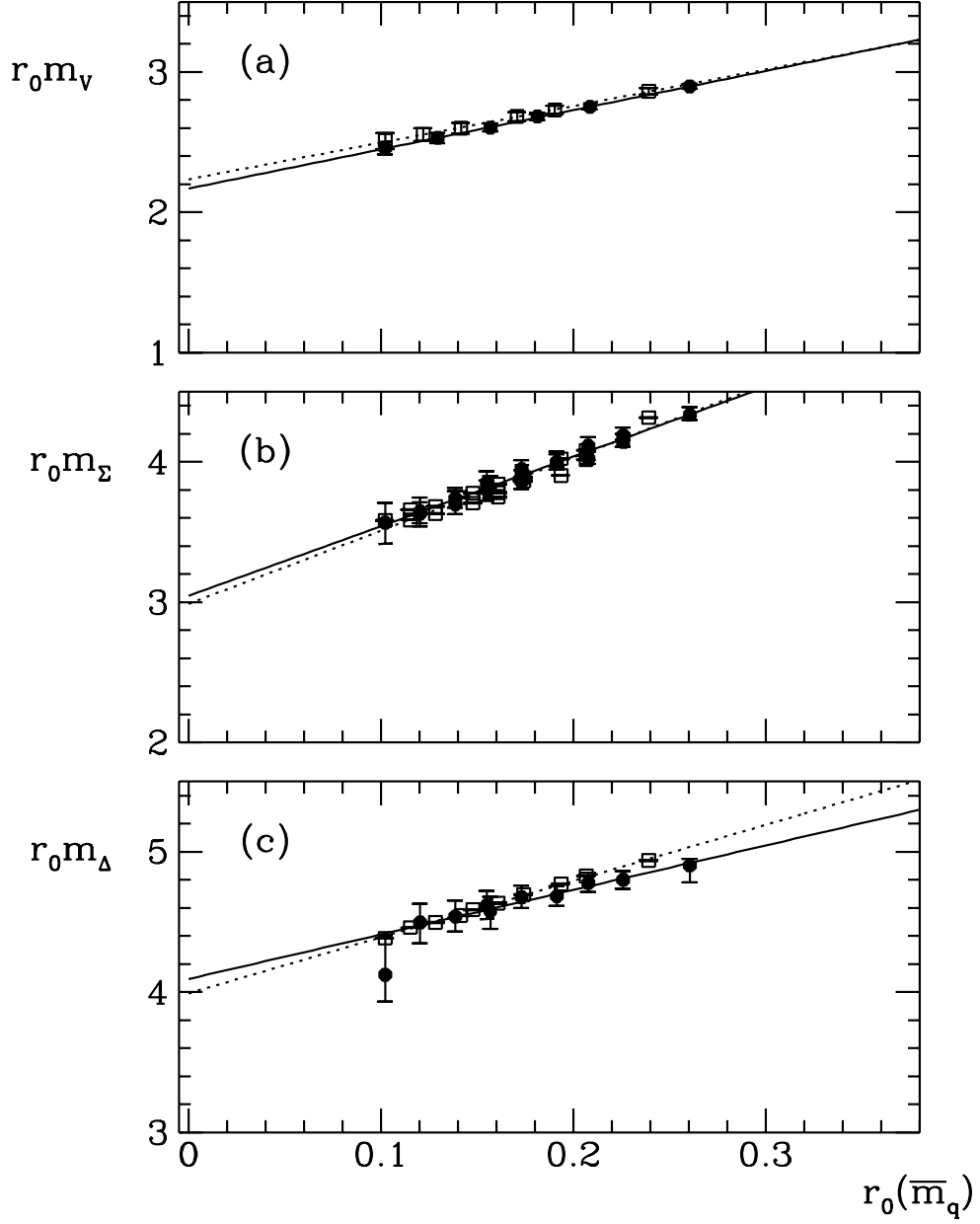


FIG. 4. Data for (a): vector mesons, (b): Σ -like baryons and (c): Δ -like baryons plotted versus the averaged quark mass $\overline{m}_q = (\tilde{m}_{q,1} + \tilde{m}_{q,2} + \tilde{m}_{q,3})/3$ in units of r_0 for the non-perturbatively improved (NP) dataset. Open squares and full circles denote the data at $\beta = 6.2$ and 6.0 , respectively. The lines represent the fits to eqs. (16–18).

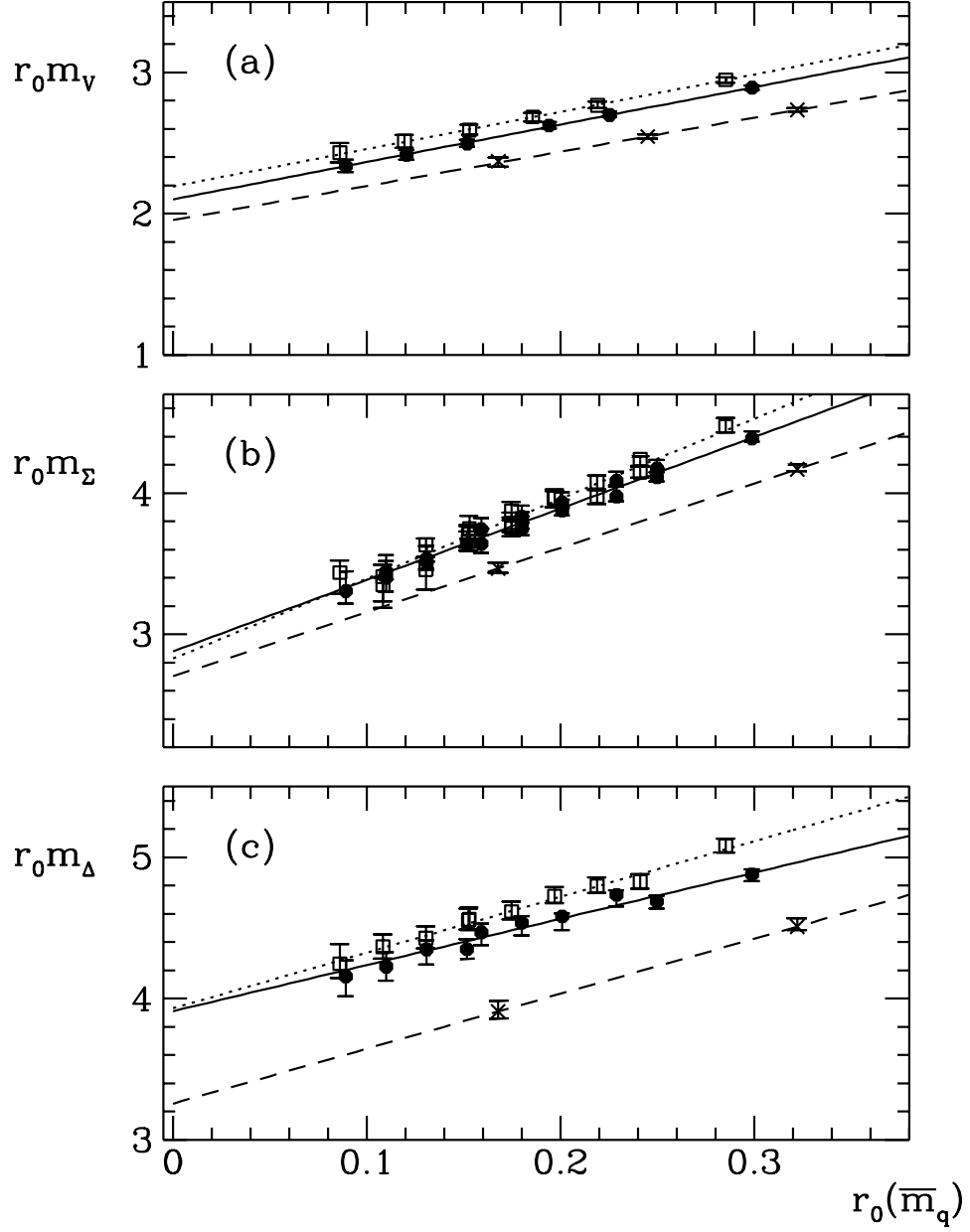


FIG. 5. Same as Fig. 4 for the TAD dataset. Open squares, full circles and crosses denote the data at $\beta = 6.2$, 6.0 and 5.7 , respectively.

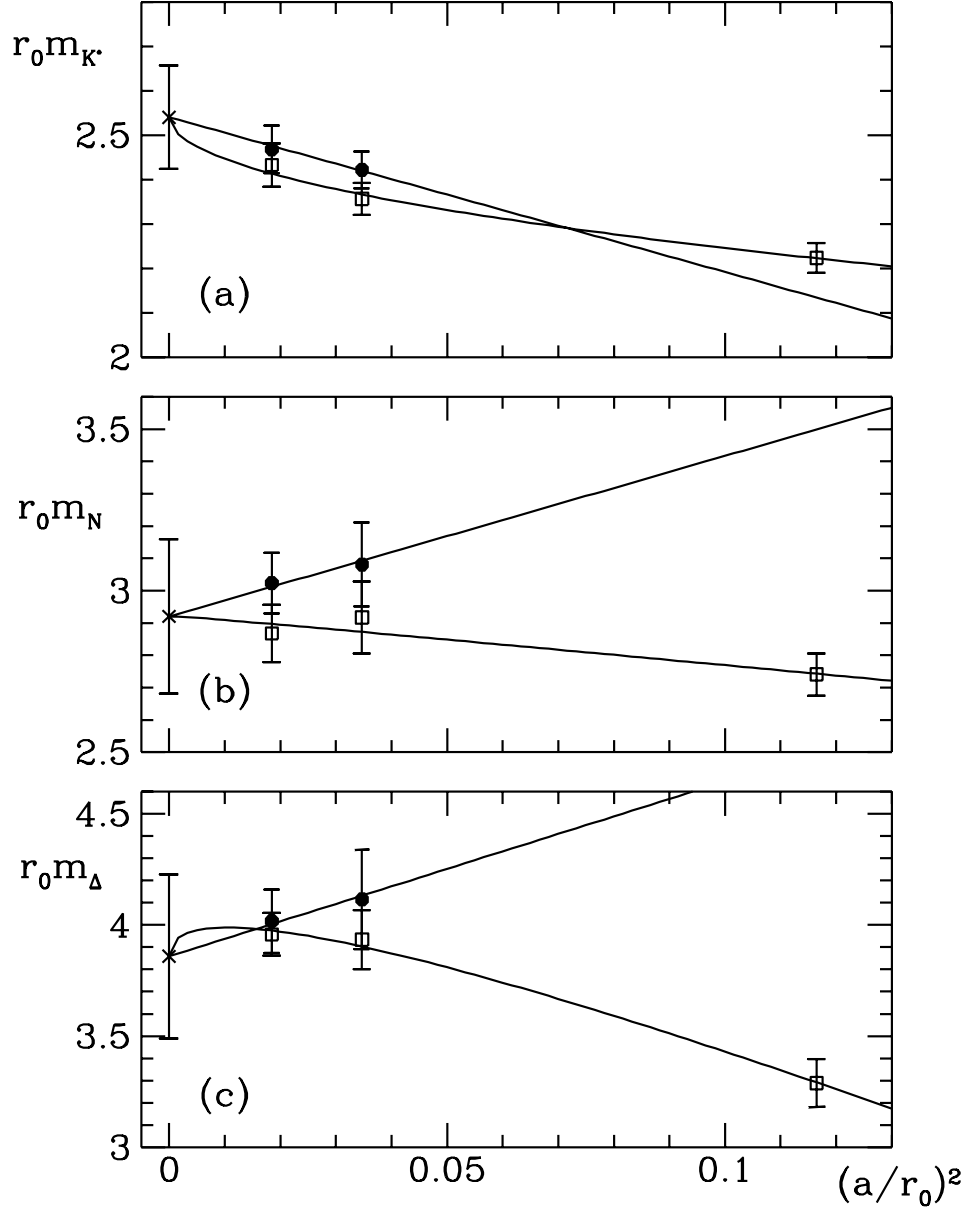


FIG. 6. Examples of simultaneous continuum extrapolations of the NP and TAD datasets. (a): the K^* meson, (b): the nucleon and (c): the Δ . Full circles denote the data computed using the non-perturbative estimate of c_{sw} , whereas the tadpole improved data are represented by open squares.

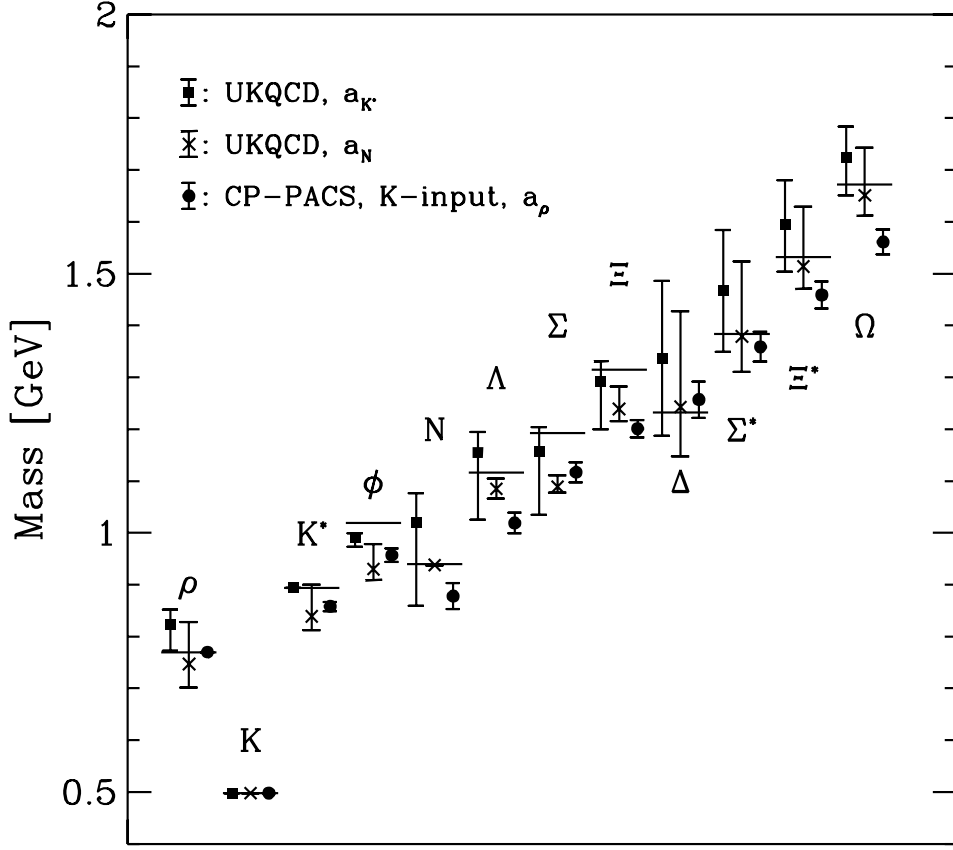


FIG. 7. The quenched light hadron spectrum computed in the $O(a)$ improved and its comparison to the results of ref. [4], obtained using the unimproved Wilson action (full circles). The levels of the experimental points are denoted by the solid lines.